The Plant Cell, Vol. 28: 1926–1944, August 2016, www.plantcell.org

Metabolite Diversity in Alkaloid Biosynthesis: A Multilane (Diastereomer) Highway for Camptothecin Synthesis in *Camptotheca acuminata*

Radin Sadre,[a] Maria Magallanes-Lundback,[a] Sujana Pradhan,[b,1] Vonny Salim,[a,1] Alex Mesberg,[a] A. Daniel Jones,[a,b] and Dean DellaPenna[a,2]

[a] Department of Biochemistry and Molecular Biology, Michigan State University, East Lansing, Michigan 48824-1319
[b] Department of Chemistry, Michigan State University, East Lansing, Michigan 48824-1319

ORCID ID: 0000-0002-8412-2579 (R.S.)

Camptothecin is a monoterpene indole alkaloid (MIA) used to produce semisynthetic antitumor drugs. We investigated camptothecin synthesis in *Camptotheca acuminata* by combining transcriptome and expression data with reverse genetics, biochemistry, and metabolite profiling. RNAi silencing of enzymes required for the indole and seco-iridoid (monoterpene) components identified transcriptional crosstalk coordinating their synthesis in roots. Metabolite profiling and labeling studies of wild-type and RNAi lines identified plausible intermediates for missing pathway steps and demonstrated nearly all camptothecin pathway intermediates are present as multiple isomers. Unlike previously characterized MIA-producing plants, *C. acuminata* does not synthesize 3-α(*S*)-strictosidine as its central MIA intermediate and instead uses an alternative seco-iridoid pathway that produces multiple isomers of strictosidinic acid. NMR analysis demonstrated that the two major strictosidinic acid isomers are (*R*) and (*S*) diastereomers at their glucosylated C21 positions. The presence of multiple diastereomers throughout the pathway is consistent with their use in synthesis before finally being resolved to a single camptothecin isomer after deglucosylation, much as a multilane highway allows parallel tracks to converge at a common destination. A model "diastereomer" pathway for camptothecin biosynthesis in *C. acuminata* is proposed that fundamentally differs from previously studied MIA pathways.

INTRODUCTION

Monoterpene indole alkaloids (MIAs) account for thousands of specialized metabolites produced by plant species from the orders Cornales and Gentianales. Much of this chemical diversity originates from the common precursor 3-α(*S*)-strictosidine, which is formed by stereospecific condensation of the indole metabolite tryptamine and the monoterpene secologanin (De Luca et al., 2014). MIA metabolic diversity likely evolved as a component of plant adaptation to changing environments and as a defensive agent against various biotic stresses. Many MIAs, including camptothecin, target specific cellular processes in mammals and have important pharmacological activities and medicinal uses. Camptothecin was first identified during the 1960s as a novel antitumor alkaloid of *Camptotheca acuminata* (Cornales), a tree native to Southern China (Wall et al., 1966). Its mode of action is the specific inactivation of topoisomerase I resulting in cell death by apoptosis (Wright et al., 2015). Semisynthetic analogs derived from camptothecin exhibit improved pharmacological properties and clinical efficacy relative to camptothecin and are widely used to treat lung, colorectal, cervical, and ovarian cancers (Liu et al., 2015). As for many alkaloids, chemical synthesis of camptothecin is impractical and the production of semisynthetic derivatives relies entirely on camptothecin isolated from the bark and seeds of *C. acuminata* and *Nothapodytes nimmoniana* (Lorence and Nessler, 2004). The increasing worldwide demand for camptothecin requires exploration of more economical and sustainable alternatives for its production.

Despite the medicinal importance of camptothecin, its biosynthesis by plants remains undeciphered. Since its original discovery in *C. acuminata*, camptothecin was found to accumulate in several Asian and African tropical and subtropical plant species from unrelated orders and families, including species of *Ophiorrhiza* (Wink, 2003; Gopalakrishnan and Shankar, 2014). Early radiolabeling experiments in *C. acuminata* demonstrated that tryptophan and its decarboxylation product tryptamine were metabolic precursors, as was a mixture of the monoterpene alcohols geraniol and its *cis*-isomer nerol, leading to classification of camptothecin as a MIA (Sheriha and Rapoport, 1976) despite it having a quinoline, and not indole, ring system. Subsequent stable isotope labeling and NMR experiments demonstrated that strictosamide served as a precursor for camptothecin in *C. acuminata* (Hutchinson et al., 1979). The co-occurrence of camptothecin in *Ophiorrhiza pumila* with the structurally related alkaloids pumiloside and deoxypumiloside suggested they are intermediates in the camptothecin biosynthetic pathway (Aimi et al., 1989). Notably, pumiloside was also detected in *C. acuminata* (Carte et al., 1990; Montoro et al., 2010). Recent studies of camptothecin biosynthesis in *O. pumila* hairy roots demonstrated that strictosidine, derived from the condensation of tryptamine and the seco-iridoid secologanin, is required for camptothecin synthesis in this species (Asano et al., 2013; Yamazaki et al., 2013).

[1] These authors contributed equally to this work.
[2] Address correspondence to dellapen@msu.edu.
The author responsible for distribution of materials integral to the findings presented in this article in accordance with the policy described in the Instructions for Authors (www.plantcell.org) is: Dean DellaPenna (dellapen@msu.edu).
www.plantcell.org/cgi/doi/10.1105/tpc.16.00193

The seco-iridoid pathway leading to strictosidine was only recently elucidated in the MIA-producing plant *Catharanthus roseus*. Geraniol 8-oxidase (CYP76B6) catalyzes hydroxylation of the MEP pathway-derived isoprenoid geraniol to 8-hydroxygeraniol, which undergoes further oxidation to the dialdehyde 8-oxogeranial (**1**) by 8-hydroxygeraniol oxidoreductase (Höfer et al., 2013). The enzyme iridoid synthase catalyzes the subsequent conversion of 8-oxogeranial (**1**) to iridodial (Geu-Flores et al., 2012), which is oxidized further to 7-deoxyloganetic acid by 7-deoxyloganetic acid synthase (CYP76A26) (Salim et al., 2014). 7-Deoxyloganetic acid is glycosylated to 7-deoxyloganic acid (Asada et al., 2013), which undergoes subsequent hydroxylation by CYP72A224 to yield loganic acid, whose carboxyl group is then *O*-methylated to form loganin (Murata et al., 2008; Salim et al., 2013). Secologanin synthase (CYP72A1) then catalyzes the oxidative ring opening of loganin to secologanin, which contains an aldehyde group suitable for condensation with the amino group of tryptamine (Irmler et al., 2000). Strictosidine synthase, a Pictet-Spenglerase, catalyzes the stereospecific condensation of tryptamine and secologanin to 3-α(*S*)-strictosidine (Bracher and Kutchan, 1992). It was proposed that strictosidine is subsequently channeled into the biosynthesis of the downstream MIAs strictosamide, pumiloside, and deoxypumiloside to yield camptothecin in *O. pumila* (Asano et al., 2013). However, poststrictosidine reaction steps, enzymes, and their sequence(s) remain unknown in camptothecin-producing plants.

The Medicinal Plant Consortium recently made the assembled transcriptome, gene expression, and metabolite profiles for *C. acuminata* publicly available (http://medicinalplantgenomics.msu.edu/, http://metnetdb.org/mpmr_public/). Here, we combined analyses of transcriptome and expression data sets with reverse genetics, biochemistry, and metabolite profiling to investigate camptothecin biosynthesis in soil-grown *C. acuminata* plants. Two essential genes for camptothecin biosynthesis, those encoding tryptophan decarboxylase and iridoid synthase, were identified and downregulated by RNAi, and the consequences for metabolite and gene expression profiles determined. Our key findings are that in contrast to other well-studied MIA producing plants, including *O. pumila* (Yamazaki et al., 2003b; Asano et al., 2013), *C. acuminata* does not synthesize strictosidine and instead uses an alternative seco-iridoid pathway to produce strictosidinic acid composed of a mixture of glucoside diastereomers varying in stereochemistry at C21. These strictosidinic acid diastereomers are channeled into the camptothecin pathway, and multiple diastereomers of other intermediates are present throughout the pathway, comparable to a multilane highway in which parallel lanes lead to a single destination, in this case a single isomer of camptothecin. Finally, we identify novel alkaloids that are plausible intermediates for missing steps in the pathway using stable isotope labeling and tandem mass spectrometry.

RESULTS

Identification and Characterization of Camptothecin Pathway Intermediates in *C. acuminata*

To assess the abundance of putative intermediates of the camptothecin pathway in *C. acuminata*, five different tissues (root, green stems, shoot apex, and young and mature leaves) were collected from wild-type plants grown under greenhouse conditions, and 70% aqueous acetonitrile extracts were subjected to nontargeted UHPLC/MS analysis using a 52-min reverse-phase chromatographic separation. Nineteen metabolites were annotated based on accurate mass measurements of positive ions and fragments observed in UHPLC/MS and UHPLC/MS/MS mass spectra (Figure 1, Table 1; Supplemental Table 1). Wild-type *C. acuminata* accumulated tryptamine (**4**), the iridoids loganic acid (**2**), and secologanic acid (**3**) as well as the MIA strictosidinic acid (**5**), but lacked detectable levels of their methyl-esterified derivatives loganin, secologanin, and strictosidine (numbers in bold numbers correspond to the chemical structures shown in Table 1 and Figure 1). This suggests that in contrast to the best studied MIA-producing plants *Rauvolfia serpentina* and *C. roseus* that use methyl-esterified intermediates (De Luca et al., 2014), *C. acuminata* uses an alternative seco-iridoid pathway with carboxylic acid intermediates up to strictosidinic acid. Several poststrictosidinic acid metabolites that we propose as intermediates in the camptothecin pathway were also detected (Table 1). In addition to the previously reported metabolites strictosamide (**6**) and pumiloside (**10**) (Hutchinson et al., 1979; Carte et al., 1990; Montoro et al., 2010), we identified metabolites with exact molecular masses and fragment ions consistent with strictosamide epoxide (**7**), strictosamide diol (**8**), strictosamide ketolactam (**9**), and deoxypumiloside (**11**) (Table 1). Surprisingly, most of these MIAs were present in multiple isomeric forms with identical exact molecular and fragment ion masses that we resolved and numbered according to their relative elution order. Note that all isomers of a compound have the same bolded number and that additional descriptors are used to differentiate isomers (e.g., isomer 1 and isomer 2). Strictosidinic acid (**5**) and strictosamide epoxide (**7**) each exhibited three isomers, while two isomers each were detected for strictosamide (**6**), strictosamide ketolactam (**9**), pumiloside (**10**), and deoxypumiloside (**11**).

We next quantified the relative levels of these metabolites and their isomers that could be detected in extracts of five different tissues for three wild-type plants (Figure 2). As expected, shoot apex and young leaf shared similar metabolite profiles and accumulated most metabolites at distinctly higher levels compared with root and/or mature leaf. Tryptamine (**4**) was only detected in stem, shoot apex, and young leaf. Loganic acid (**2**) content was highest in stem, lower in other photosynthetic tissues, and absent from root. Secologanic acid (**3**) was detected in all five tissues with levels in photosynthetic tissues 2- to 3-fold higher than in roots. The major accumulation sites for strictosidinic acid (**5**) were shoot apex and young leaf with progressively lower levels in stem, root, and mature leaf. Surprisingly, the levels of strictosamide (**6**) were nearly identical in all tissues. Strictosamide epoxide (**7**), strictosamide diol (**8**), and strictosamide ketolactam (**9**) could not be reliably quantified due to their low abundances in all *C. acuminata* tissues. The tissue distribution profile of pumiloside (**10**) was similar to that of strictosidinic acid (**5**), with the highest levels being in shoot apex and young leaf and lowest levels in mature leaf. Deoxypumiloside (**11**) was only detected in stem, root, and at extremely low levels in shoot apex. All tissues contained camptothecin (**12**) with young leaf and shoot apex accumulating the highest levels. It is noteworthy that the relative amounts of isomers of strictosidinic acid (**5**) and poststrictosidinic acid intermediates

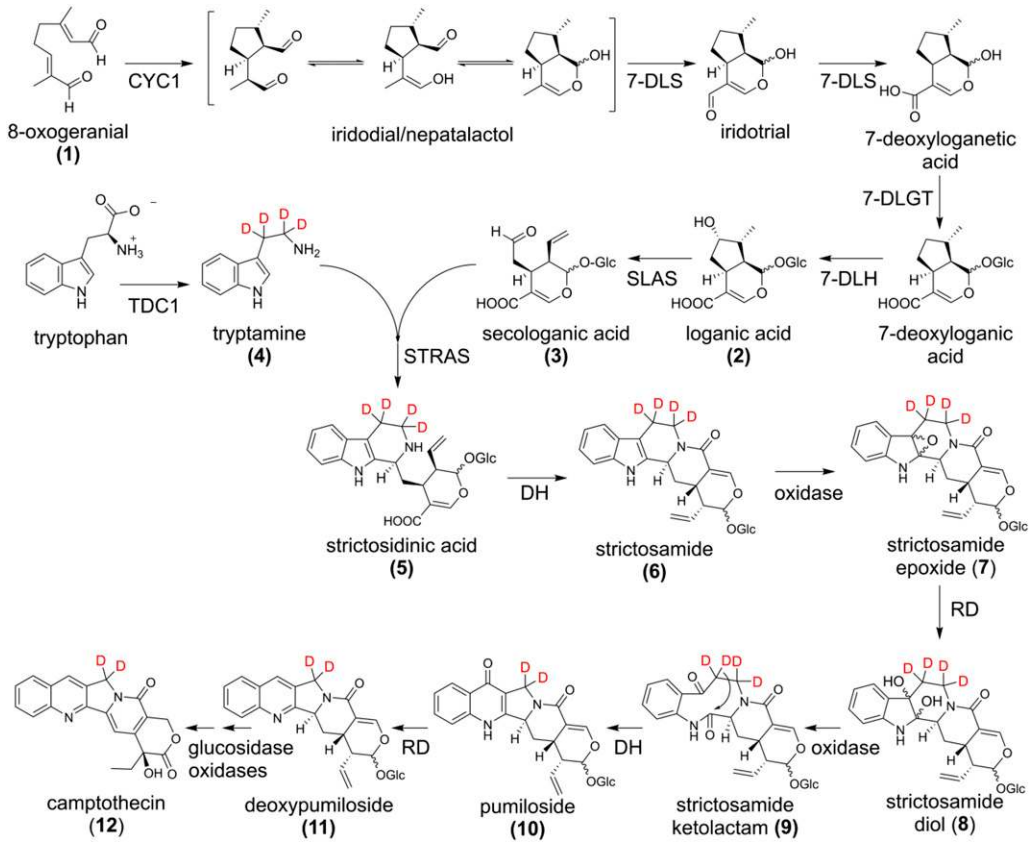

Figure 1. Proposed Pathway for Camptothecin Biosynthesis in *C. acuminata*.

Camptothecin (**12**) is synthesized from the central precursor strictosidinic acid (**5**) derived from condensation of tryptamine (**4**) and the iridoid secologanic acid (**3**), a monoterpenoid glycoside. In vivo labeling experiments with deuterated [α,α,β,β-d_4]-tryptamine resulted in labeling of strictosidinic acid and downstream metabolites with the number and the likely positions of deuterium (D) indicated in red. Enzyme activities are indicated. TDC1 and CYC1 were identified and characterized in this study. 7-DLS, 7-deoxyloganetic acid synthase; 7-DLGT, 7-deoxyloganetic acid glucosyltransferase; 7-DLH, 7-deoxyloganic acid hydroxylase; SLAS, secologanic acid synthase; STRAS, strictosidinic acid synthase; DH, dehydration; RD, reduction.

varied among tissues (Figure 2). In most tissues, one of the two major isomers was more abundant; for example, strictosamide (**6**) isomer 1 predominates in roots and stems, while isomer 2 predominates in shoot apices and leaves. In general, roots and stems have similar isomer profiles as do young and mature leaves.

The presence of multiple isomeric MIA metabolites in UHPLC/MS metabolite profiles of *C. acuminata* tissues with indistinguishable MS/MS spectra (Table 1; Supplemental Table 1) suggested they differ in stereochemical configurations, but their chromatographic resolution indicates they are diastereomers. To assess the nature of these isomeric compounds, the two most abundant isomers of strictosidinic acid (**5**), which were present in sufficient quantity to be purified, were subjected to an assortment of one- and two-dimensional NMR spectroscopic analyses. The most substantial differences were observed in the ^{1}H chemical shifts at position 21 (Table 2; Supplemental Data Set S1), which is the position of glycosylation. Subsequent coupled heteronuclear single quantum coherence (cHSQC) NMR spectra were generated to assess whether relative stereochemical configuration of hydrogens at chiral positions could be assessed by measuring the ^{1}H-^{13}C coupling constants, which are sensitive to orientation relative to other bonds and have been used to establish relative bond orientations in a variety of metabolites (Marquez et al., 2001). These coupling constants ($^{1}J_{C\text{-}H}$) were 170 Hz for isomer 2 and 178 Hz for isomer 3, the largest isomer-related difference among all $^{1}J_{C\text{-}H}$ values and consistent with two epimers differing in the stereochemistry of C-glycosylation at position 21 (Figure 3, Table 2). Based on similarities to NMR spectra reported for 21(*S*)-strictosidine, we assign strictosidinic acid isomer 3 to have the 21(*R*) configuration and strictosidinic acid isomer 2 to have 21(*S*) configuration (Figure 3), the latter being in common with the published structure and coupling constants of 21(*S*)-strictosidine (Patthy-Lukáts et al., 1997). NMR data for stereocenters at positions 3, 15, and 20 and the carbohydrate resonances for isomers 2 and 3 did not differ substantially, consistent with the difference being the configuration at position 21. These two diastereomer configurations are most likely formed earlier in iridoid biosynthesis by the spontaneous ring opening and closing of 7-deoxyloganetic acid that forms C2-hydroxy epimers, which are then glycosylated (Figure 4). The presence of multiple isomers for most of the

Table 1. Relevant Compounds Detected in Wild-Type *C. acuminata*

Annotated Metabolite	Formula	Retention Time (min)	Calculated *m/z* for $[M+H]^+$	Experimental Precursor *m/z* for $[M+H]^+$	Fragment Ion(s) Observed in MS/MS Spectra (*m/z*)	*TDC1*-RNAiNo. of Deuterium Atoms
Tryptamine (**4**)	$C_{10}H_{12}N_2$	8.0	161.1079	161.1065	144	4
Loganic acid (**2**)	$C_{16}H_{24}O_{10}$	13.6 (2 isomers)[a]	377.1448	377.1450	359, **215**, 197, 179, 161, 151, 137, 133, 123, 109, 81	0
Secologanic acid (**4**)	$C_{16}H_{22}O_{10}$	15.1 (2 isomers)[a]	375.1291	375.1290	**213**, 195, 177, 151, 125, 109, 107, 95, 79, 77	0
Strictosidinic acid (**5**)	$C_{26}H_{32}N_2O_9$	23.9 (isomer 1) 24.8 (isomer 2) 26.5 (isomer 3)	517.2186	517.2198	500, **355**, 338, 320, 269/268, 251, 194, 180/181, 168/170, 151, 156, 144, 130, 125	n.d. (isomer 1) 4 (isomer 2) 4 (isomer 3)
Strictosamide (**6**)	$C_{26}H_{30}N_2O_8$	37.6 (isomer 1) 41.5 (isomer 2)	499.2080	499.2081	**337**, 319, 267, 171, 144	4 (isomer 1) 4 (isomer 2)
Strictosamide epoxide (**7**)	$C_{26}H_{30}N_2O_9$	22.8 (isomer 1) 24.8 (isomer 2) 26.5 (isomer 3)	515.2030	515.2021	**353**, 335, 309, 291, 283, 265, 263, 237, 209, 183, 184, 155, 144	n.d. (isomer 1) n.d. (isomer 2) n.d. (isomer 3)
Strictosamide diol (**8**)	$C_{26}H_{32}N_2O_{10}$	20.1	533.2135	533.2170	**371**, 353, 283, 265, 185, 160, 142, 132	n.d.
Strictosamide ketolactam (**9**)	$C_{26}H_{30}N_2O_{10}$	22.5 (isomer 1) 22.7 (isomer 2)	531.1979	531.1953	**369**, 351, 341, 299, 281, 271, 253, 194, 176, 158, 148, 130, 124, 106	n.d. (isomer 1) n.d. (isomer 2)
Pumiloside (**10**)	$C_{26}H_{28}N_2O_9$	30.2 (isomer 1) 32.9 (isomer 2)	513.1873	513.1890	**351**, 333, 315, 305, 281, 235, 140	2 (isomer 1) n.d. (isomer 2)
Deoxypumiloside (**11**)	$C_{26}H_{28}N_2O_8$	36.1 (isomer 1) 38.2 (isomer 2)	497.1924	497.1930	**335**, 265, 247, 219, 183, 169, 142, 97	2 (isomer 1) 2 (isomer 2)
Camptothecin (**12**)	$C_{20}H_{16}N_2O_4$	34.3	349.1188	349.1198	305, 277, 249, 219/220, 168	2

Metabolites in root, stem, shoot apex, and leaf extracts were separated by a 52-min UHPLC/MS/MS method and are listed with their precursor and fragment ions. Fragment ions obtained after loss of a glucose unit (162 D) are highlighted in bold. Only stem tissue contained detectable levels of all metabolite isomers listed here. The last column in the table summarizes the results of in vivo labeling experiments with [α,α,β,β-d_4]-tryptamine in *TDC1*-RNAi plants, which do not accumulate tryptamine-derived MIAs without tryptamine supplementation. After incubation of *TDC1*-RNAi apical cuttings with [α,α,β,β-d_4]-tryptamine for 6 weeks, several deuterated MIAs were detectable in stem extracts. The number of deuterium atoms incorporated into detectable metabolites is indicated in the last column, with n.d. indicating compounds that were below the limit of detection in deuterium labeling experiments.

[a]Loganic acid and secologanic acid exist also as multiple isomers that were not resolved with this UHPLC/MS method but were resolved using a different chromatography system (Supplemental Figures 1 and 2).

later biosynthetic intermediates suggests that *C. acuminata* 7-deoxyloganetic acid glucosyltransferase is either a promiscuous enzyme that can accommodate both *R*- and *S*-isomers of 7-deoxyloganetic acid or that multiple stereospecific *C. acuminata* 7-deoxyloganetic acid glycosyltransferases exist. Under our 52-min chromatographic conditions, the first iridoids we can detect, loganic acid (**2**) and secologanic acid (**3**), appeared as single chromatographic peaks; however, two isomers were resolved for each using a different chromatography column and gradient (Supplemental Figures 1 and 2). Thus, the isomers observed throughout the pathway are likely glucosidic isomers that have their origin early in iridoid synthesis.

On the basis of these observations, a model pathway for camptothecin synthesis in *C. acuminata* is proposed (Figure 1), where tryptamine (**4**) and the aldehyde-containing iridoid secologanic acid (**3**) (rather than secologanin) are coupled via a Pictet-Spengler reaction, leading to strictosidinic acid (**5**). Intramolecular dehydrative cyclization of strictosidinic acid yields strictosamide (**6**). Conversion of the indole ring system to the quinoline ring is postulated to occur via multistep oxidation to strictosamide ketolactam (**9**) followed by condensation and elimination of water to yield the quinolinone ring of pumiloside (**10**). The subsequent reduction to deoxypumiloside (**11**), deglycosylation, and other metabolic conversions lead to the end product camptothecin (**12**). This model pathway takes into account the formation and retention of multiple glycosidic isomers (diastereomers) for pathway intermediates from 7-deoxyloganetic acid to deoxypumiloside (**11**).

Identification of Candidate Genes Involved in Camptothecin Biosynthesis

Genes responsible for the production of camptothecin in *C. acuminata* are largely unknown. A previous study demonstrated that *C. acuminata* possesses two differentially expressed tryptophan decarboxylase genes, *TDC1* and *TDC2*, for the synthesis of tryptamine (López-Meyer and Nessler, 1997). Transcriptome data from the Medicinal Plant Genomics Resource (MPGR) database (Góngora-Castillo et al., 2012) indicated that *TDC1* expression is moderate to high in leaves, roots, and young bark of *C. acuminata*, while *TDC2* transcript is barely detectable in most plant tissues, with the exception of immature and mature fruit. In mature leaves, roots, and young bark, *TDC1* transcript levels are

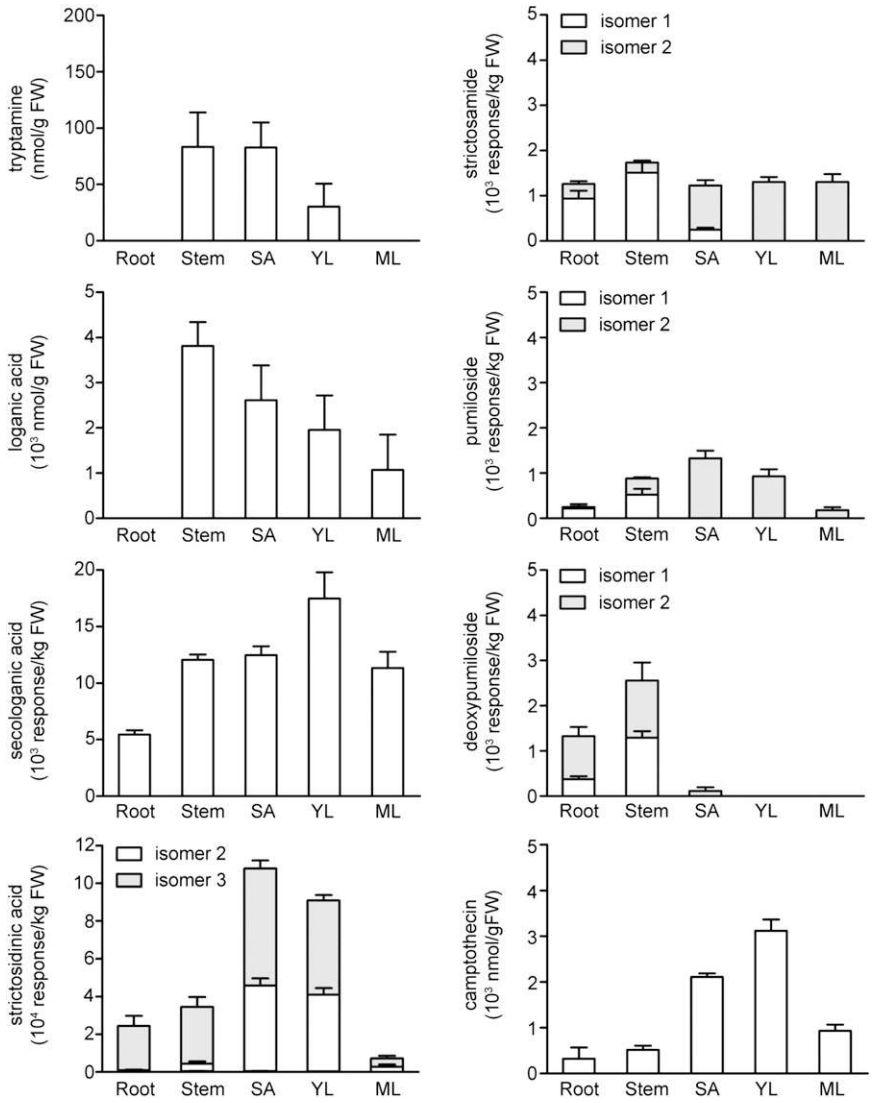

Figure 2. Tissue Distribution Profiles of Proposed Camptothecin Pathway Metabolites in Wild-Type *C. acuminata*.

Tissues were collected from wild-type plants that had been under greenhouse cultivation in soil for 8 months and 70% acetonitrile extracts were analyzed using a 15-min gradient elution method for UHPLC/MS. Multiple isomers were detected for strictosidinic acid (Figure 1, compound **5**) and poststrictosidinic acid metabolites (Figure 1, compounds **6**, **10**, **11**, and **12**). Average values are shown with SD ($n = 3$) for the most abundant and quantifiable isomers. SA, shoot apex; YL, young leaf; ML, mature leaf.

100-, 200-, and 600-fold, respectively, higher than *TDC2* transcript levels. Since *TDC1* is expressed in tissues that accumulate camptothecin, we considered it the most promising candidate for synthesizing the indole precursor of camptothecin. The predicted TDC1 protein shares 68 and 74% sequence identities with the tryptophan decarboxylases of *C. roseus* (De Luca et al., 1989) and *O. pumila* (Yamazaki et al., 2003a), respectively.

To select additional candidate camptothecin biosynthesis genes, the MPGR transcriptome data were used for coexpression analyses. We postulated that seco-iridoid pathway genes would be coexpressed with *TDC1* to coordinate synthesis of the seco-iridoid and indole precursors needed for camptothecin production. The original MPGR data set included developmental and tissue-specific expression profiles for 53,154 unique *C. acuminata* transcripts in 18 tissues from different developmental stages such as 10-d-old seedlings to fruiting trees (Góngora-Castillo et al., 2012). Prior to coexpression analysis, genes exhibiting low transcript abundances ($\log_2$ fragments per kilobase of transcript per million mapped reads [FPKM] lower than 2) in root or immature bark were removed from the data set, leaving 26,874 unique transcripts for further analyses. Additionally, as iridoid synthesis is known to involve cyclization, oxidation, and glycosylation reactions (Miettinen et al., 2014), 1146 transcripts encoding putative proteases, histone and histone-modifying proteins, ribosomal proteins, tRNA synthetases, and proteins related to ubiquitinylation were considered unlikely to have direct involvement in

Table 2. NMR Chemical Shifts and Coupling Constants for Strictosidinic Acid Isomers Isolated from *C. acuminata* Leaf Tissue as Measured from J-Resolved ^{1}H Spectra and ^{1}H-^{13}C cHSQC Spectra

Carbon number and group	^{1}H shift (ppm) and $^{3}J_{H-H}$ coupling constants (Hz)	^{13}C shift (ppm) and $^{1}J_{C-H}$ coupling constants (Hz)	^{1}H shift (ppm) and $^{3}J_{H-H}$ coupling constants (Hz)	^{13}C shift (ppm) and $^{1}J_{C-H}$ coupling constants (Hz)
	Isomer 2		Isomer 3	
3 (CH)	4.45 (dd), ^{3}J = 3.4, 7.7 Hz	50.8, ^{1}J = 144 Hz	4.56 (dd), ^{3}J = 3.6, 7.9 Hz	53.1, ^{1}J = 143 Hz
5 (CH_2)	3.29 (m) 3.75 (m)	41.3, ^{1}J = 143, 145 Hz;	3.45 (m) 3.50 (m)	39.6, ^{1}J = 139, 141 Hz
6 (CH_2)	3.01 (m) 3.29 (m)	18.1, ^{1}J = 131, 133 Hz	2.99 (m) 3.04 (m)	18.2, ^{1}J = 129, 131 Hz
9 (CH)	7.56 (d), ^{3}J = 7.9 Hz	117.7, ^{1}J = 159 Hz	7.55 (d), ^{3}J = 7.9 Hz	117.6, ^{1}J = 158 Hz
10 (CH)	7.15, ^{3}J = 7.4 Hz	119.1, ^{1}J = 159 Hz	7.13, ^{3}J = 7.3 Hz	118.9, ^{1}J = 158 Hz
11 (CH)	7.23, ^{3}J = 7.6 Hz	121.9, ^{1}J = 159 Hz	7.23, ^{3}J = 7.6 Hz	121.8, ^{1}J = 158 Hz
12 (CH)	7.42, ^{3}J = 8.2 Hz	110.7, ^{1}J = 159 Hz	7.45, ^{3}J = 8.2 Hz	110.8, ^{1}J = 158 Hz
14 (CH_2)	2.15 (dd), ^{3}J = 4.6, 11.1 Hz; 2.40 (dd), ^{3}J = 5.9, 11.6 Hz	33.7, ^{1}J = 128, 129 Hz	1.98 (m) 2.46 (m)	34.1, ^{1}J = 130, 131 Hz
15 (CH)	3.00 (m)	32.6, ^{1}J = 137 Hz	2.96 (m)	32.9, ^{1}J = 135 Hz
17 (CH)	7.67 (s)	151.7, ^{1}J = 191 Hz	7.35 (s)	148.4, ^{1}J = 192 Hz
18 (CH_2)	5.32 (d), ^{3}J = 10.7 Hz; 5.43 (d), ^{3}J = 17.3 Hz	117.5, ^{1}J = 155, 158 Hz	5.39 (d), ^{3}J = 11.0 Hz; 5.47 (d), ^{3}J = 17.3 Hz	118.4, ^{1}J = 154, 161 Hz
19 (CH)	5.96 (dd), ^{3}J = 10.3, 17.5 Hz	134.8, ^{1}J = 156 Hz	6.19 (dd), ^{3}J = 10.2, 17.2 Hz	134.8, ^{1}J = 152 Hz
20 (CH)	2.70 (m)	44.2, ^{1}J = 134 Hz	2.74 (m)	44.9, ^{1}J = 132 Hz
21 (CH)	**5.93 (d), ^{3}J = 9.5 Hz**	**95.1, ^{1}J = 170 Hz**	**5.64 (d), ^{3}J = 8.2 Hz**	**95.5, ^{1}J = 178 Hz**
1′ (CH)	4.92 (d), ^{3}J = 8.0 Hz	98.9, ^{1}J = 163 Hz	4.85 (d), ^{3}J = 7.9 Hz	98.8, ^{1}J = 162 Hz
2′ (CH)	3.44 (m)	76.5, ^{1}J = 145 Hz	3.41 (m)	76.5, ^{1}J = 145 Hz
3′ (CH)	3.41 (m)	77.3, ^{1}J = 145 Hz	3.35 (m)	77.3, ^{1}J = 145 Hz
4′ (CH)	3.26 (m)	70.2, ^{1}J = 145 Hz	3.28 (m)	70.3, ^{1}J = 145 Hz
5′ (CH)	3.24 (m)	73.3, ^{1}J = 145 Hz	3.24 (m)	73.3, ^{1}J = 145 Hz
6′ (CH_2)	3.68 (dd), ^{3}J = 4.95, 12.2 Hz; 4.12 (dd), ^{3}J = 2.17, 12.1 Hz	61.6, ^{1}J = 141, 142 Hz	3.76 (dd), ^{3}J = 6.61, 12.3 Hz; 4.05 (dd), ^{3}J = 2.40, 12.6 Hz	61.5, ^{1}J = 131, 132 Hz

Notable differences in ^{1}H chemical shifts and $^{1}J_{C-H}$ coupling constants were observed for position 21 (highlighted in bold in the table).

specialized metabolism and were also removed, leaving a data set of 25,725 transcripts for hierarchical cluster analyses.

Hierarchical cluster analysis identified a subcluster of 23 transcripts that encode seven proteins with highest identity to known steps in the seco-iridoid pathway. These include geraniol-8-oxidase (G8O), CYCLASE1 (CYC1), and CYC2, which are members of the progesterone 5-β-reductase family, 7-deoxyloganetic acid synthase, and glucosyltransferase, a putative ortholog of the *C. roseus* iridoid transcription factor bHLH IRIDOID SYNTHESIS1 (BIS1) (Van Moerkercke et al., 2015), along with a putative ortholog to protein S, an α/β-hydrolase superfamily protein associated with seco-iridoid/MIA synthesizing cells in *C. roseus* (Leménager et al., 2005) (Figure 5). Like *TDC1*, most of the seco-iridoid pathway candidate genes in this cluster showed moderate to high expression in root and immature bark, but they also had lower expression than *TDC1* in other tissues (e.g., mature leaf), which

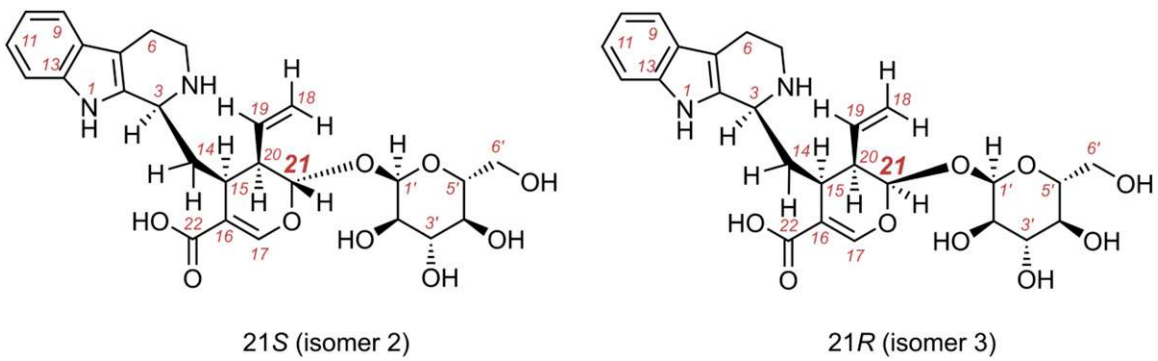

Figure 3. Structures of the Two Major Strictosidinic Acid Isomers Isolated from *C. acuminata* Leaf Tissue.

NMR analyses (Table 2) show that the two major strictosidinic acid isomers (isomers 2 and 3) differ in stereochemical configuration at position C21, the site of glucosylation.

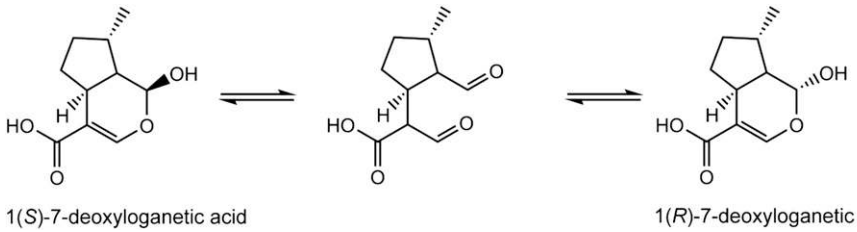

Figure 4. Formation of Iridoid Diastereomers.

Equilibrium between the open and closed ring conformations of 7-deoxyloganetic acid yields diastereomers at the C2 hydroxyl group.

resulted in their clustering apart from *TDC1* (Figure 4). The tryptophan and MEP pathways provide substrates from intermediary metabolism for tryptamine and iridoid synthesis, respectively. To assess whether members of these pathways have expression patterns similar to that of the iridoid cluster, *C. acuminata* transcripts encoding steps of the tryptophan and MEP pathways were identified by homology searches (Supplemental Data Set S2), and their expression profiles subjected to hierarchical cluster analysis together with transcripts of the iridoid subcluster (Supplemental Figure 3 and Supplemental Data Set S3). This

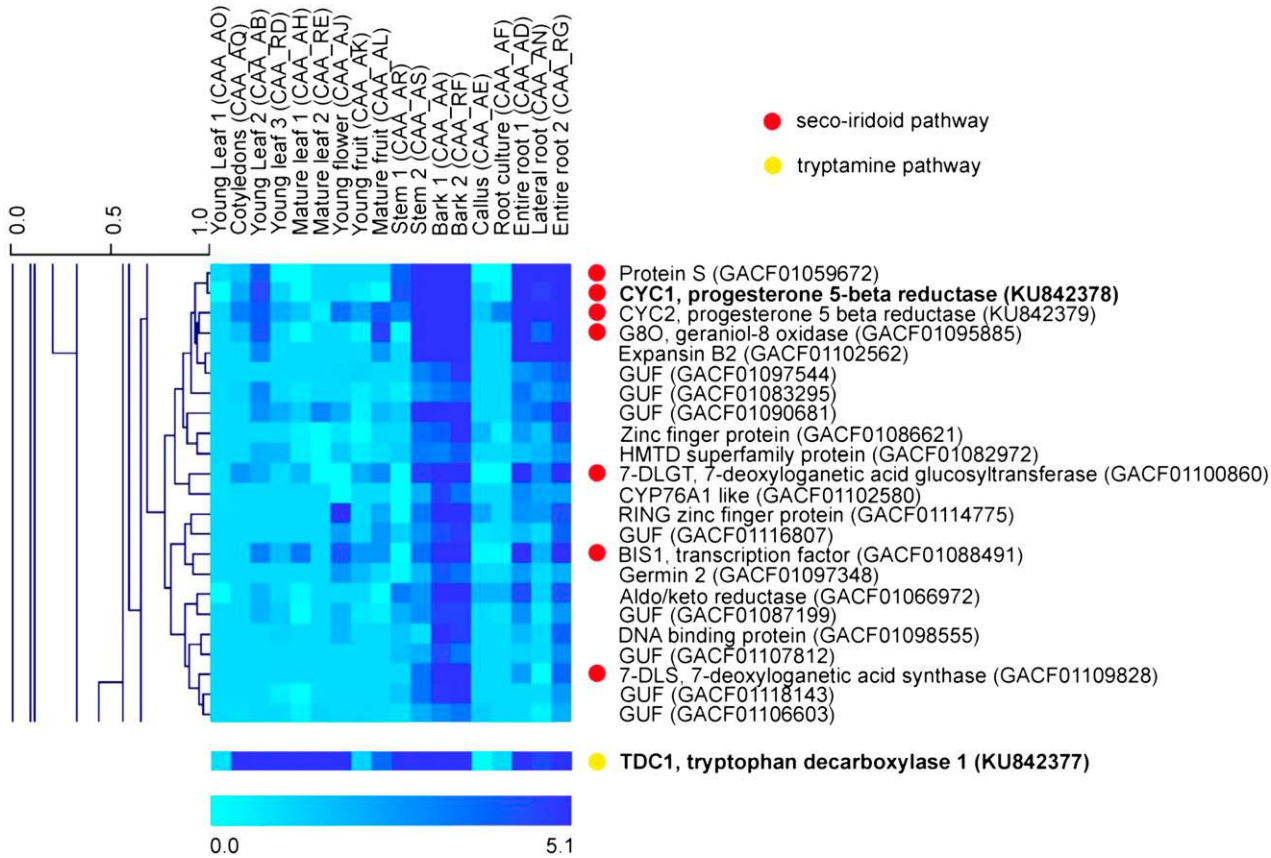

Figure 5. Heat Map of Expression Data of Candidate Genes for the Seco-Iridoid Branch of Camptothecin Biosynthesis.

Hierarchical clustering of 25,725 transcripts was generated based on average linkage of Pearson correlation coefficients of $\log_2$-transformed FPKM expression values from the MPGR website (http://medicinalplantgenomics.msu.edu/) with MeV v4.9 (Saeed et al., 2006). A subcluster encompassing 23 genes is shown with GenBank accession numbers listed in parentheses. The color scale depicts transcript abundance (expressed as $\log_2$-transformed FPKM). Red dots indicate the position of candidates for the seco-iridoid pathway, and for comparison, the expression profile (expressed as $\log_2$-transformed FPKM) of *TDC1* is shown (yellow dot). *CYC1* and *TDC1*, both highlighted in bold, have been characterized in this study. Note that lists of candidate genes, GenBank accession numbers, MPGR transcript identifiers, and FPKM values are given in Supplemental Data Sets 2 and 3. HMTD, heavy metal transport/detoxification; GUF, gene of unknown function.

analysis showed that the expression pattern of most tryptophan and MEP pathway genes is quite different from that of the iridoid subcluster, with a few notable exceptions: one gene encoding a tryptophan synthase subunit and one gene encoding an anthranilate synthase subunit.

CYC1 Shows Iridoid Synthase Activity in Vitro

In *C. roseus*, iridoid synthase is a member of the progesterone 5-β-reductase family that catalyzes the NAD(P)H-dependent conversion of 8-oxogeranial (**1**) to iridodial/nepetalactol in MIA biosynthesis (Geu-Flores et al., 2012; Munkert et al., 2015). This suggested that one or both of the *C. acuminata* progesterone 5-β-reductase family members in our gene cluster (Figure 5, CYC1 and CYC2) might encode orthologous iridoid synthase activities in camptothecin biosynthesis. The *C. acuminata* transcriptome encodes at least seven progesterone 5-β-reductase family members, of which *CYC1* and *CYC2*, with 65 and 59% amino acid sequence identity, respectively, have the highest identities to *C. roseus* iridoid synthase. In comparative analysis of the phylogenetic relationships between predicted members of the progesterone-5-β-reductase family in *C. roseus*, *C. acuminata*, and *R. serpentina*, CYC1 and CYC2 formed separate, well-resolved clades (Supplemental Figure 4 and Supplemental Data Set S4).

To examine the catalytic activities of CYC1 and CYC2 in comparison to the previously characterized *C. roseus* iridoid synthase (Geu-Flores et al., 2012), the respective coding sequences were expressed in *Escherichia coli* and recombinant His-tagged proteins purified by affinity chromatography. The purified enzymes were subsequently tested in colorimetric dehydrogenase assays for protein functionality that are based on the NAD(P)H-dependent reduction of nitroblue tetrazolium chloride to the dark-blue formazan product. These experiments indicated that all three enzymes were functional and required NAD(P)H as cofactor for activity (Supplemental Figure 5). The purified proteins were then assayed for iridoid synthase activity with 8-oxogeranial (**1**) as substrate using a chemically synthesized substrate (Geu-Flores et al., 2012) composed of a mixture of the *cis-trans* isomers 8-oxogeranial (**1**)/8-oxoneral in an approximate 2:1 ratio. Incubation of CYC1 with substrate and NADPH resulted in nearly complete conversion of the substrate to seven *cis-trans* isomers of iridodial/nepetalactol that were indistinguishable in gas chromatographic retention times and mass spectra to those obtained with the *C. roseus* iridoid synthase control (Figure 6). These data clearly demonstrated that like *C. roseus* iridoid synthase, *C. acuminata* CYC1 catalyzes the reductive cyclization of 8-oxogeranial (**1**). Assays with CYC2 did not result in any detectable products, indicating that CYC2 may not use 8-oxogeranial (**1**) as substrate in planta (Figure 6).

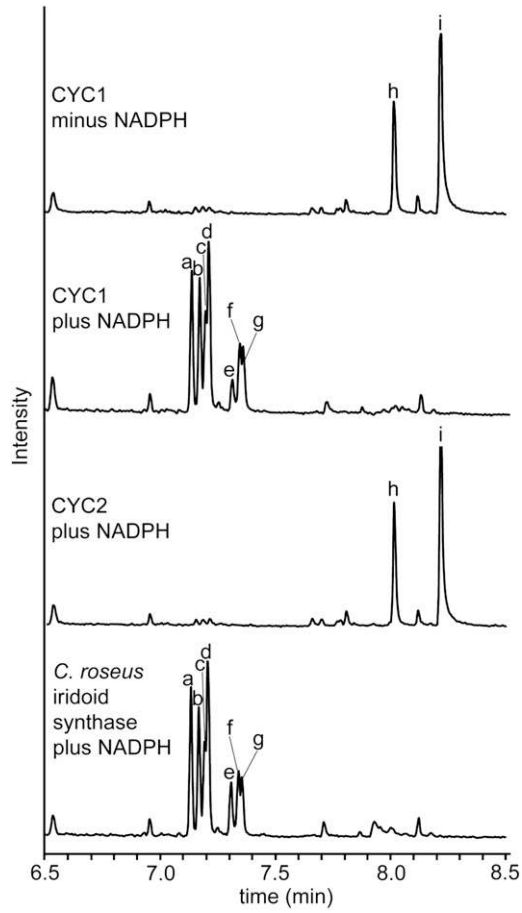

Figure 6. Iridoid Synthase Assay with Recombinant CYC1 and CYC2 Enzymes.

Purified recombinant proteins were assayed for iridoid synthase activity in reaction mixtures with 8-oxogeranial (Figure 1, compound **1**) in the absence or presence of NADPH. Assays were extracted with dichloromethane and analyzed by GC/MS. The respective total ion chromatograms are shown in comparison to that obtained for a control assay with *C. roseus* iridoid synthase (**a** to **g**, reaction products; **h** and **i**, 8-oxoneral and 8-oxogeranial substrates, respectively). In the presence of NADPH, CYC1 and *C. roseus* iridoid synthase catalyzed conversion of the substrate to reduction products while no products were detectable in assays with CYC2. Incubation of the proteins in reaction mixtures lacking NADPH did not result in detectable products; CYC1 minus NADPH is shown as a representative trace.

Silencing of *CYC1* and *TDC1* Expression in *C. acuminata* Plants

CYC1 and *TDC1* were selected as targets for reverse genetics analyses by gene silencing. We developed a stable transformation method to integrate RNAi-mediating expression cassettes into the *C. acuminata* genome using the pHellsgate12 system (Helliwell and Waterhouse, 2005). *C. acuminata* cotyledon explants were transformed by *Agrobacterium tumefaciens* harboring RNAi constructs for *TDC1* or *CYC1* and transgenic plants were regenerated in vitro. Rooted antibiotic-resistant plantlets were transferred from in vitro culture to soil cultivation under greenhouse conditions. With the exception of decreased resistance to red spider mite infestation, RNAi plants did not show any obvious phenotypic differences compared with wild-type plants (Supplemental Figure 6).

After a growth and acclimation period of 3 to 4 months under greenhouse cultivation, RNAi-mediated suppression of the target genes was evaluated in independent transformation events by quantitative real-time PCR. Since *TDC1* and *CYC1* expression in wild-type plants is highest in immature bark, stem tissue was used

to determine mRNA abundances for target genes in RNAi plants relative to untransformed wild-type control plants. In the six *TDC1*-RNAi plants analyzed, *TDC1* stem transcript levels were decreased to as low as 3% of wild-type levels (Figure 7A). Consistent with this observation, camptothecin levels in mature leaves of *TDC1*-RNAi plants were reduced by as much as 1000-fold compared with wild-type plants (Figure 7A). Similar analyses were performed on nineteen *CYC1*-RNAi plants where a much wider range of silencing and impact on leaf camptothecin levels was observed (Figure 7B). Approximately half of the *CYC1*-RNAi lines had stem *CYC1* transcript levels below 15% of the wild type. This group of *CYC1*-RNAi lines also had 15- to 400-fold lower camptothecin levels in mature leaves than did wild-type plants. Taken together, these data indicate that stable RNAi transformation was successful in *C. acuminata* and that the expression of both *TDC1* and *CYC1* are necessary for camptothecin biosynthesis.

Target gene impact was further examined in five independent transformed lines of *TDC1*-RNAi and *CYC1*-RNAi that had severely reduced mature leaf camptothecin levels and three wild-type lines independently regenerated through tissue culture. Plants used for these studies had been under greenhouse cultivation for about eight months. RNA was extracted from roots, green stems, and young developing leaves, and the average *TDC1* and *CYC1* mRNA levels were compared (Figure 8). In wild-type plants, *TDC1* transcript levels were ~2-fold higher in stems than roots and young leaves and barely detectable in these tissues in *TDC1*-RNAi lines (Figure 8A). *CYC1* expression in wild-type plants was highest in stems and ~40-fold that of roots and young leaves (Figure 8B). The average *CYC1* mRNA level in green stems of *CYC1*-RNAi lines was strongly reduced to 4% of the wild type, while in roots and young leaves, it was only reduced to 49 and 27% of wild-type levels, respectively, suggesting that target-gene silencing was less effective in these two tissues (Figure 8B).

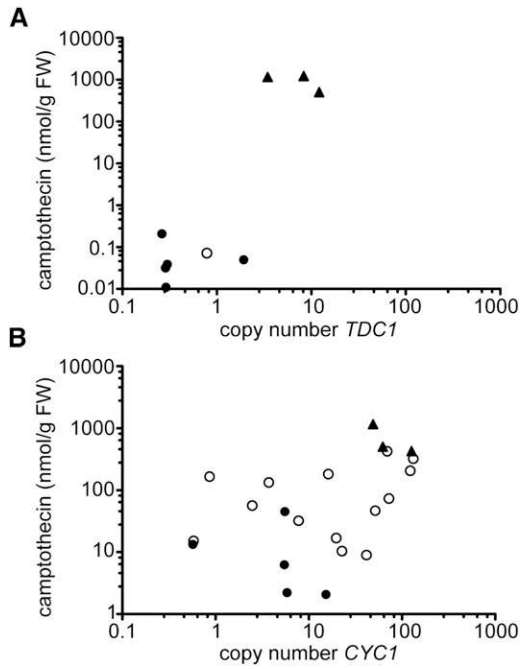

Figure 7. Correlation Analyses between Stem Transcript Abundance of the RNAi-Targeted Gene with the Mature Leaf Camptothecin Content of Transgenic RNAi Plants and Wild-Type Plants.

Data are shown for *TDC1*-RNAi plants **(A)** and for *CYC1*-RNAi plants **(B)** in comparison to wild-type plants (filled triangles). Each circle represents one RNAi plant from an independent transformation event, with filled circles indicating lines that were selected for further in-depth analyses. For the wild type, three independent lines were taken through tissue culture and regeneration. Stems and mature leaves were collected from plants that had been under greenhouse cultivation in soil for approximately 4 months. Note that the values are plotted on double $\log_{10}$ scale.

TDC1-RNAi Plants Are Deficient in Indole Alkaloids and Accumulate Loganic Acid in Roots

To further evaluate the impact of *TDC1* gene silencing on camptothecin biosynthesis, extracts from roots, stems, shoot apices, and young and mature leaves were subjected to UHPLC/MS analyses. In contrast to the wild-type controls, *TDC1*-RNAi lines did not accumulate detectable levels of tryptamine (**4**), strictosidinic acid (**5**), or any of the poststrictosidinic acid metabolites in Figure 1, including the newly proposed pathway intermediates strictosamide epoxide (**7**), strictosamide diol (**8**), and strictosamide ketolactam (**9**). By contrast, the levels of the iridoids loganic acid (**2**) and secologanic acid (**3**) in stems, shoot apices, and leaves of *TDC1*-RNAi plants were not significantly different from wild-type levels (Figure 9). However, all *TDC1*-RNAi lines accumulated loganic acid (**2**) in roots, a metabolite below detection in wild-type roots (Figure 9).

To assess whether the absence of strictosidinic acid (**5**) and poststrictosidinic acid metabolites in the *TDC1*-RNAi lines was directly attributable to tryptamine (**4**) deficiency, feeding experiments with deuterated tryptamine were performed. Apical cuttings from *TDC1*-RNAi and wild-type plants were incubated in aqueous solutions with or without tryptamine-$\alpha,\alpha,\beta,\beta$-$d_4$. After 6 weeks, stems and mature leaves were collected and extracts prepared and analyzed via UHPLC/MS. As expected, incubation of wild-type apical cuttings with deuterated tryptamine resulted in little incorporation of label into camptothecin pathway intermediates due to the substantial intrinsic pool of unlabeled tryptamine in stem and shoot apex (~100 nmol per gram fresh weight; Figure 2). However, when *TDC1*-RNAi cuttings were incubated with deuterated tryptamine, deuterium-labeled camptothecin pathway intermediates were detected in stems and to a lesser extent in leaves. Four deuterium atoms from tryptamine-d_4 were incorporated into strictosidinic acid (**5**) isomers 2 and 3 and strictosamide (**6**) isomers 1 and 2, while two deuterium atoms were incorporated into pumiloside (**10**) isomer 1, deoxypumiloside (**11**) isomers 1 and 2, and camptothecin (**12**), providing further evidence for the role of these metabolites as intermediates in camptothecin synthesis (Table 1). Because the absolute levels of all pathway compounds in deuterated tryptamine *TDC1*-RNAi cuttings were still much lower than in wild-type cuttings, incorporation of label into less abundant isomers could not be reliably determined. The likely positions of deuterium labels within the different pathway intermediates are indicated in Figure 1.

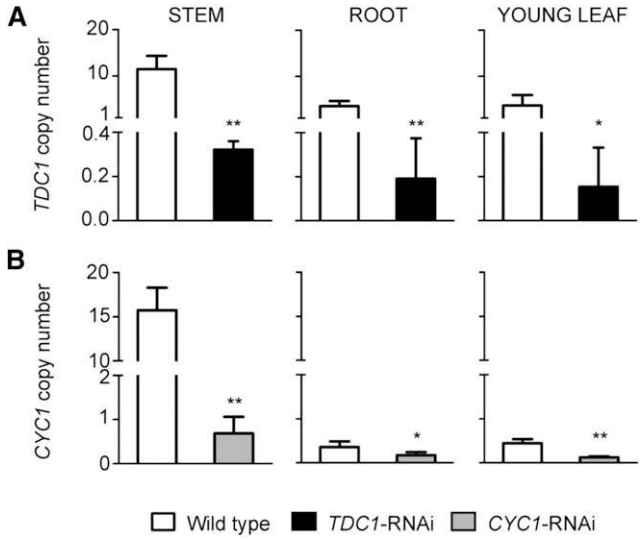

Figure 8. Expression Analyses of the RNAi-Targeted Gene in Root, Young Stems, and Young Leaves of *TDC1*-RNAi Plants and *CYC1*-RNAi Plants Relative to the Wild Type.

Tissues were collected from plants that had been under greenhouse cultivation for 8 months. Average transcript copy numbers were normalized to *ACTIN6* mRNA ($n = 5$ and 3 for RNAi and wild-type plants, respectively) and are shown for *TDC1*-RNAi plants **(A)** and *CYC1*-RNAi plants **(B)** relative to the wild type. Note that the *y* axis is discontinuous to allow depiction of the significant differences in RNAi target gene copy numbers between wild-type and RNAi lines. Asterisks indicate significant differences in RNAi plants (unpaired *t* test; *$P < 0.05$; **$P < 0.001$) relative to the wild type.

Impaired Indole Alkaloid Biosynthesis in *CYC1*-RNAi Plants Is Accompanied by Increased Tryptamine Levels

We similarly assessed the impact of *CYC1*-RNAi by analyzing pathway metabolite levels in roots, stems, shoot apices, and young and mature leaves of five independent *CYC1*-RNAi lines in comparison to the wild type. In addition to a sharp reduction in camptothecin levels in all tissues to as low as 2% of wild-type levels, all tissues of *CYC1*-RNAi lines accumulated substantially higher levels of tryptamine (**4**) compared with the wild type (Figure 9). In contrast to wild-type and *TDC1*-RNAi plants, which lacked detectable levels of tryptamine in roots and mature leaves, *CYC1*-RNAi roots and mature leaves contained ~250 nmol tryptamine per gram fresh weight (Figure 9). In stems, shoot apices, and young leaves of the *CYC1*-RNAi lines, tryptamine levels approached or exceeded 1000 nmol per gram fresh weight (15- to 23-fold increases relative to the wild type).

None of the *CYC1*-RNAi lines accumulated detectable levels of loganic acid (**2**) in any tissue, and in most tissues, the levels of secologanic acid (**3**), strictosidinic acid (**5**), and the post-strictosidinic acid intermediates were also reduced at least 6-fold relative to the wild type (Figure 9, Table 3), with strictosamide epoxide (**7**), strictosamide diol (**8**), and strictosamide ketolactam (**9**) levels being reduced to below the detection limit. With regard to the isomer composition of strictosidinic acid (**5**) and post-strictosidinic acid metabolites, the levels of all identified isomers were decreased in *CYC1*-RNAi lines relative to those in the wild type, in some tissues to below the detection limit (Table 3). Isomer compositions were also radically altered in certain tissues of the *CYC1*-RNAi lines compared with average wild-type levels. For example, strictosidinic acid (**5**) was composed of 39% isomer 2 [21(*S*) isomer] and 61% isomer 3 [21(*R*) isomer] in mature leaves of the wild type, whereas in *CYC1*-RNAi lines, isomer 3 was more dominant (94%). Strictosamide (**6**) in roots and stems of the wild type consisted mainly of isomer 1 (74 and 87%, respectively), while isomer 2 was exclusively accumulated in *CYC1*-RNAi lines. Pumiloside (**10**) in stems of the wild type was composed of 41% isomer 2, whereas in *CYC1*-RNAi lines, pumiloside isomer 1 was the only detectable isomer. Surprisingly, deoxypumiloside (**11**) isomer compositions did not significantly differ between wild-type and *CYC1*-RNAi plants. These combined results for the impact of *CYC1*-RNAi are consistent with the metabolite profiles of *TDC1*-RNAi lines and the proposed pathway for camptothecin biosynthesis (Figures 1 and 9).

Transcriptional Crosstalk between the Indole and Iridoid Biosynthetic Pathways

To test whether indole and iridoid precursor synthesis might be coordinated, we analyzed the expression of additional candidate genes in RNAi plants compared with the wild type. *CYC1*, *CYC2*, and *G8O* (geraniol-8-oxidase; Figure 5) mRNA levels were determined and compared in the roots and green stems of *TDC1*-RNAi and wild-type plants (Figure 10). All three genes were expressed most highly in stems (Figures 10B and 10D), with *CYC2* mRNA levels not being significantly different in any genotype or tissue. However, in *TDC1*-RNAi roots, *CYC1* and *G8O* mRNA levels were increased 9- and 40-fold, respectively, relative to the wild type (Figure 10A), suggesting that in response to the severe reduction in tryptamine and camptothecin biosynthesis (Figure 9) the monoterpene branch of the pathway is specifically upregulated in roots of *TDC1*-RNAi plants. *CYC1*-RNAi lines with strong impact on *CYC1* expression and mature leaf camptothecin levels were similarly assessed for *TDC1*, *CYC2*, and *G8O* expression (Figures 10C and 10D). While *G8O* and *CYC2* transcript levels were not significantly different between *CYC1*-RNAi lines and wild-type plants, *TDC1* expression was significantly increased 3-fold in roots (Figure 10C), suggesting that in response to the severe reduction in levels of monoterpene intermediates (Figure 9, Table 3) and camptothecin biosynthesis in *CYC1*-RNAi lines, the indole branch is upregulated. These data indicate the existence of a transcriptional crosstalk mechanism between the indole and the iridoid branch of the camptothecin pathway in *C. acuminata* roots.

DISCUSSION

The *C. acuminata* Seco-Iridoid Pathway Generates Isomeric, Acidic Precursors for Camptothecin Biosynthesis

Our results indicate that *C. acuminata* (order Cornales) uses a seco-iridoid pathway that fundamentally differs from that in *C. roseus* and *R. serpentina*, two plant species in the order Gentianales in which seco-iridoid and MIA synthesis has been most extensively studied (De Luca et al., 2014). *C. roseus* and

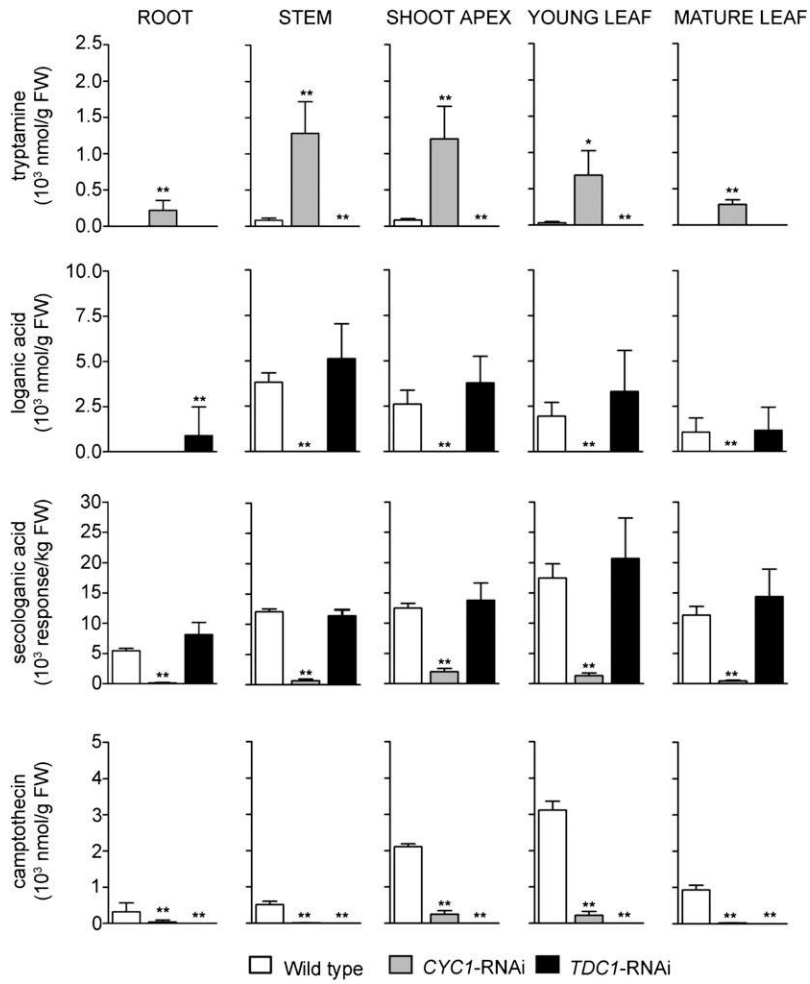

Figure 9. Levels of Tryptamine, Loganic Acid, Secologanic Acid, and Camptothecin in Different Tissues of Wild-Type *C. acuminata* and *CYC1*-RNAi and *TDC1*-RNAi Plants.

Tissues were collected from plants that had been under greenhouse cultivation for 8 months. Average levels of tryptamine, loganic acid, secologanic acid, and camptothecin (Figure 1, compounds 4, 2, 3, and 12, respectively) are shown with SD for wild-type ($n = 3$), *CYC1*-RNAi ($n = 5$), and *TDC1*-RNAi lines ($n = 5$). Asterisks indicate significantly different metabolite levels in *CYC1*-RNAi lines and *TDC1*-RNAi (unpaired *t* test; *$P < 0.05$; **$P < 0.001$) relative to the wild type.

R. serpentina form the methyl esters loganin and secologanin to produce the key MIA precursor strictosidine. These compounds are absent from *C. acuminata* and, instead, the carboxylic acids loganic acid (**2**) and secologanic acid (**3**) accumulate and are utilized to synthesize strictosidinic acid (**5**) (Table 1). In this regard, *C. acuminata* also differs from *O. pumila*, the only other camptothecin-producing species for which some biochemical and molecular data exist. Like *C. roseus* and *R. serpentine*, *O. pumila* is also in the order Gentianales and utilizes methyl ester intermediates to produce strictosidine (Asano et al., 2013). Consistent with this, protein extracts from *O. pumila* tissues showed strictosidine synthase activity, while those from *C. acuminata* leaves, stems, and root tissues lacked this activity (Yamazaki et al., 2003b). These combined data indicate that at least two routes for camptothecin have evolved in plants, a "Gentianales-type" pathway exemplified by *O. pumila* and a novel pathway in *C. acuminata* (Figure 1) that is identical to the "Gentianales-type" seco-iridoid pathway only up through loganic acid formation and thereafter uses carboxylic acid, instead of methyl ester, intermediates (Asano et al., 2013; Miettinen et al., 2014; Salim et al., 2014).

In *C. acuminata*, tryptamine (**4**) is condensed with secologanic acid (**3**) to form strictosidinic acid (**5**), instead of with secologanin to form strictosidine as in the order Gentianales. Moreover, plant species of the order Gentianales form a single isomer of strictosidine as the initial MIA intermediate (Asano et al., 2013; Miettinen et al., 2014), while *C. acuminata* produces a mixture of strictosidinic acid (**5**) isomers as its initial MIA intermediate (Figures 2 and 3, Table 3). NMR analyses of the two major strictosidinic acid isomers (isomers 2 and 3) show that they differ in stereochemical configuration (are diastereomers) at position C21, the site of glucosylation (Figure 3, Table 2). These data suggest that all iridoids in the pathway leading to strictosidinic acid are also present as isomeric mixtures. Prior to glucosylation, equilibrium between

Table 3. Isomer Compositions of Strictosidinic Acid and Poststrictosidinic Acid Metabolites in Different Tissues of *CYC1*-RNAi Lines Compared to the Wild Type

		Wild Type					*CYC1*-RNAi				
Metabolite	Isomer	Root	Stem	Shoot Apex	Young Leaf	Mature Leaf	Root	Stem	Shoot Apex	Young Leaf	Mature Leaf
Strictosidinic acid	**1**	n.d.	447 ± 147	475 ± 87	342 ± 54	n.d.	n.d.	n.d.**	130 ± 116**	42 ± 58**	n.d.
	2	997 ± 298	3,970 ± 1,098	45,252 ± 3,958	40,524 ± 3,540	2,808 ± 1,220	155 ± 112**	1,025 ± 822*	3,436 ± 1,811**	2,742 ± 884**	2,070 ± 733
	3	23,477 ± 5,219	30,066 ± 5,284	62,147 ± 4,213	50,004 ± 2,840	4,400 ± 1,379	3,020 ± 1,826**	1,209 ± 712**	8,022 ± 4,086**	2,381 ± 1,108**	49 ± 67**
Strictosamide	**1**	936 ± 175	1,511 ± 264	249 ± 41	n.d.	n.d.	n.d.**	n.d.**	n.d.**	n.d.	n.d.
	2	323 ± 65	222 ± 24	975 ± 121	1,305 ± 107	1,306 ± 170	165 ± 74*	21 ± 13**	125 ± 35**	132 ± 35**	149 ± 127**
Pumiloside	**1**	219 ± 90	520 ± 130	n.d.	n.d.	n.d.	n.d.**	152 ± 90*	n.d.	n.d.	n.d.
	2	28 ± 11	360 ± 25	1,329 ± 167	928 ± 153	179 ± 65	n.d.**	n.d.**	127 ± 45**	n.d.**	n.d.**
Deoxypumiloside	**1**	373 ± 66	1,291 ± 141	n.d.	n.d.	n.d.	63 ± 61**	372 ± 169**	n.d.	n.d.	n.d.
	2	955 ± 203	1,266 ± 395	111 ± 88	n.d.	n.d.	165 ± 85**	436 ± 108*	n.d.	n.d.	n.d.

Tissues were collected from plants grown under greenhouse cultivation for 8 months and metabolite levels determined by UHPLC/MS. Average levels expressed as response per kilogram fresh weight are shown with SD for biological replicates. For the wild type, three plants independently derived from tissue culture were analyzed and for *CYC1*-RNAi lines, and five plants from independently derived transgenic events were analyzed. Asterisks indicate significantly different metabolite levels in *CYC1*-RNAi lines (unpaired *t* test; *$P < 0.05$; **$P < 0.001$) relative to the wild type. n.d., below the limit of quantification, which is defined as signal/noise = 10.

the open-ring and closed-ring conformations of 7-deoxyloganetic acid yields stereoisomers at the C2 carbon atom (Figure 4), both of which are subsequently glucosylated (Figure 1). This proposed mechanism is consistent with the detection of two isomers for loganic acid (**2**) and secologanic acid (**3**) (Supplemental Figures 1 and 2) as well as the presence of isomer mixtures for strictosidinic acid (**5**) and most poststrictosidinic acid intermediates (Table 1).

Silencing of two essential genes for synthesis of the monoterpene and indole components of camptothecin, *CYC1* and *TDC1*, respectively, provide strong evidence for the involvement of specific metabolites in the proposed camptothecin pathway in *C. acuminata*. *CYC1* RNAi lines with low *CYC1* transcript levels had levels of the iridoid loganic acid reduced to below detection and significantly lowered levels of secologanic acid compared with the wild type (Figure 9). Additionally, the levels and isomers of all strictosidinic acid (**5**) and poststrictosidinic acid intermediates (including camptothecin) were significantly decreased in *CYC1*-RNAi lines relative to the wild type (Figure 9, Table 3). These data are consistent with the iridoid synthase activity of CYC1 in vitro (Figure 6) and with CYC1 being the major, and possibly only, iridoid synthase involved in camptothecin synthesis in *C. acuminata*. Silencing of *TDC1* greatly impaired the plants' production of tryptamine (**4**) and all indole-containing intermediates/isomers of the proposed camptothecin pathway (Figure 9). Additional evidence for the indole-dependent synthesis of various strictosidinic acid (**5**) and poststrictosidinic acid isomers was obtained by feeding experiments with *TDC1*-RNAi apical cuttings, where deuterated tryptamine was incorporated into many of the proposed intermediates and their isomers, including camptothecin (Table 1). Most significantly, *TDC1*-RNAi and *CYC1*-RNAi lines impacted, to different degrees, the same strictosidinic acid (**5**) and poststrictosidinic acid intermediates/isomers.

Combining nontargeted metabolite analyses in the wild type with metabolite profiling in RNAi lines allowed us to identify new pathway intermediates of extremely low abundance in the wild type (i.e., strictosamide epoxide, diol, and ketolactam) that are consistent with the biosynthetic scheme shown in Figure 1. These three novel metabolites are likely formed from isomeric strictosamide (**6**), yielding first strictosamide epoxide (**7**) that is further converted to strictosamide diol (**8**) and then to its ketolactam (**9**), which undergoes intramolecular cyclization of enolate to carbonyl, followed by dehydration, in a manner similar to the well known aldol condensation. This process channels strictosamide (**6**) toward pumiloside (**10**) synthesis by completing the quinolone ring topology that provides the framework for camptothecin. In the proposed pathway, pumiloside isomers are then reduced to deoxypumiloside (**11**) isomers. Although the sequential order of subsequent metabolic conversions that resolve the diastereomers at carbon-21 to the single stereochemistry in camptothecin has not been established, it is evident from the chemistry that deglucosylation and oxidations are involved. After deglucosylation, these final reactions convert the chiral sp^3 carbon-21 to a sp^2 carbon and eliminate the chirality at the C-atom site of glucosylation. Notably, deglucosylation of *R* and *S* diastereomers leads to formation of an aglucone whose ring can again spontaneously open and close, just as in nonglucosylated iridoids (Figures 1 and 4). Later oxidation of the ring C-atom to a carbonyl

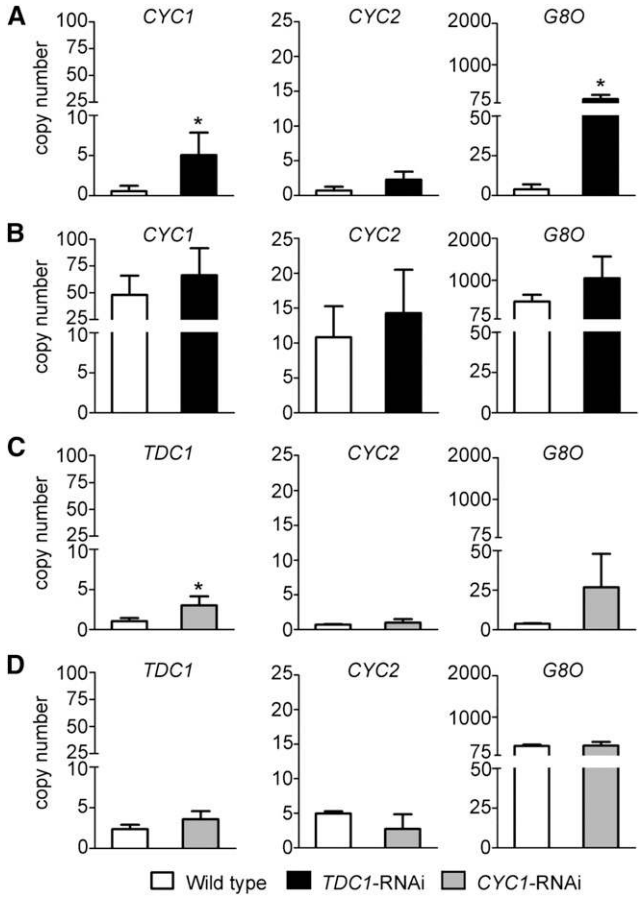

Figure 10. Root and Stem Expression of Pathway Genes Not Targeted by RNAi in *TDC1*-RNAi and *CYC1*-RNAi Plants in Comparison to the Wild Type.

Tissues were collected from RNAi plants that had been under greenhouse cultivation for 8 months. mRNA levels for *CYC1*, *CYC2*, and *G8O* in roots **(A)** and stems **(B)** of *TDC1*-RNAi and wild-type plants are shown. Root **(C)** and stem **(D)** transcript levels, respectively, for *TDC1*, *CYC2*, and *G8O* in *CYC1*-RNAi plants compared with the wild type. Average transcript copy numbers were normalized to *ACTIN6* mRNA for RNAi and wild-type plants ($n = 5$ and 3, respectively). Asterisks indicate significant differences in RNAi plants in comparison to the wild type (unpaired *t* test; *$P < 0.05$). Note that the *y* axis scales for *CYC2* and *G8O* are different from *CYC1* and *TDC1*.

C-atom "fixes" the closed ring conformation and hence determines the single stereochemistry present in camptothecin.

The abundance of glucoside isomer mixtures for the majority of the camptothecin biosynthetic pathway, from loganic acid (**2**) to deoxypumiloside (**11**), is both remarkable and unprecedented in MIA biosynthesis. This has profound implications from a mechanistic perspective because it suggests that some, if not all, of the enzymes from 7-deoxyloganetic acid to deoxypumiloside (**11**) are able to accommodate multiple isomers or that multiple enzymes exist for each step that are specific for a single stereoisomer. Given that the metabolic transformations from strictosidinic acid (**5**) to deoxypumiloside (**11**) are remote from the site of glycosylation, the consistent presence of multiple intermediate isomers in this portion of the pathway suggests that a single enzyme could accommodate both stereoisomer substrates. However, the variation in the isomeric composition of strictosidinic acid (**5**) and poststrictosidinic acid compounds between different tissues in the wild type as well as the marked changes in the isomer composition of certain metabolites in some *CYC1*-RNAi tissues (Table 3) indicate that additional stereoselective sinks or processes are active in *C. acuminata*.

Genetic Evidence for the Alternative Seco-Iridoid Pathway in *C. acuminata*

Besides CYC1, additional candidates for the early steps of the *C. acuminata* seco-iridoid pathway formed a tight 23 transcript "seco-iridoid" cluster in transcriptome-wide coexpression analyses (Figure 5). This cluster includes transcripts encoding proteins with high sequence identities (65 to 78%) to *C. roseus* geraniol synthase (Kumar et al., 2015), G8O (Höfer et al., 2013), CYC1 (Geu-Flores et al., 2012), 7-deoxyloganetic acid synthase (Salim et al., 2014), and glucosyltransferase (Asada et al., 2013) (Figure 5) and BIS1, a bHLH transcription factor that regulates iridoid synthesis in *C. roseus*. CYC2 is also in this cluster but is not likely to be involved in camptothecin biosynthesis as it lacks iridoid synthase activity in vitro (Figure 5) and, despite still being coordinately expressed with CYC1, was unable to compensate for loss of CYC1 activity in *CYC1*-RNAi lines (Figures 9 and 10). This cluster also included two transcripts encoding proteins that could conceivably contribute to iridoid and/or camptothecin production in *C. acuminata*, an aldo/keto reductase and protein S, an α/β-hydrolase superfamily protein associated with MIA synthesizing cells in *C. roseus* (Leménager et al., 2005). With the exception of a CYP76A1 transcript, other transcripts are genes of unknown function or homologous to proteins inconsistent with a role in the pathway. Finally, in contrast to the high identity of early iridoid pathway enzymes in *C. acuminata* and *C. roseus*, the last two steps of the seco-iridoid pathway in *C. roseus*, secologanin synthase (a P450), and strictosidine synthase lack obvious orthologs in the *C. acuminata* transcriptome (several transcripts with ~50 and 37% identities, respectively; Supplemental Data Set S2). These low identities may be a reflection of their different substrates in the two species: *C. acuminata* enzymes using ionizable, carboxylic acid intermediates, while *C. roseus* substrates are the equivalent nonionizable methyl esters. The fact that none of these low identity secologanin and strictosidine synthase candidates are present in the "seco-iridoid" cluster suggests the latter portion of seco-iridoid synthesis in *C. acuminata* is at minimum not coregulated with its earlier steps. This is likely also true for poststrictosidinic acid steps of the pathway as, with the exception of a CYP76A1 and an aldo/keto reductase, the "seco-iridoid" cluster also lacks additional transcripts predicted to encode the reductases, oxidases, or glucosidases postulated to carry out poststrictosidinic acid steps (Figure 1).

The extreme diversity of monoterpene indole alkaloids in nature raises fundamental questions about evolution of the pathway, especially in light of the data presented here for *C. acuminata*. Synthesis of loganic acid has been documented for numerous other plant species from unrelated plant orders and families (Skaltsounis et al., 1989; Müller and Weigend, 1998; Rastrelli et al.,

1998; Graikou et al., 2002; Han et al., 2008; Serrilli et al., 2008; Aberham et al., 2011; Zhang et al., 2012; Asano et al., 2013; Zhou et al., 2013; Fan et al., 2014), and it appears to represent a trait that arose relatively early in plant evolution. The highly conserved proteins for early seco-iridoid biosynthesis in the unrelated species *C. acuminata* and *C. roseus* are consistent with this interpretation. By contrast, the differences in seco-iridoid biosynthesis that yield exclusively strictosidinic acid in *C. acuminata* (Cornales) and strictosidine in the Gentianales (*C. roseus*, *R. serpentina*, and *O. pumila*) indicate that postloganic acid steps likely evolved later. In this context, it must be mentioned that although *C. roseus*, *R. serpentina*, and *O. pumila* all produce exclusively strictosidine, several other members of the Gentianales, most notably other *Ophiorrhiza* species, are able to produce strictosidinic acid (Arbain et al., 1993; Hamzah et al., 1994; Reanmongkol et al., 2000; Cardoso et al., 2004; Itoh et al., 2008; Ajala et al., 2011; Farias et al., 2012). As additional biochemical and genetic information is not available for these strictosidinic acid-producing Gentianales, a comparison of them with *C. roseus* and *C. acuminata* is not possible but would help clarify if strictosidinic acid arose independently (i.e., by convergent evolution) or whether the lack of secologanic acid methylation in *C. acuminata* is an ancestral trait.

Where Is Camptothecin Biosynthesis Located in *C. acuminata*?

The compartmentalization of alkaloid biosynthesis is remarkably diverse and complex across the plant kingdom with various studies demonstrating localization of distinct steps to specific organelles, cell types, tissues, and organs (Ziegler and Facchini, 2008; Courdavault et al., 2014; De Luca et al., 2014; Bedewitz et al., 2014). In this regard, it is apparent from expression profiles (Figures 5 and 10; Supplemental Data Set S3) that *TDC1* and *CYC1* and other early seco-iridoid candidate genes are expressed most highly in stems and roots of wild-type *C. acuminata*, suggesting these two tissues are particularly important sites for synthesis of indole and seco-iridoid precursors. Indeed, wild-type stems exhibited the highest *TDC1*, *G8O*, and *CYC1* transcript levels (Figures 8 and 10) and high levels of tryptamine, loganic acid, and secologanic acid (Figure 2). Stems were also the only wild-type tissue that contained detectable levels of all the metabolites and isomers reported in this study, including the low abundance intermediates strictosamide epoxide (**7**), diol (**8**), and ketolactam (**9**), which is consistent with stem playing a key role in the synthesis of poststrictosidinic acid metabolites. Finally, in labeled tryptamine feeding experiments, *TDC1*-RNAi stems accumulated the largest number of labeled metabolites, including camptothecin, further supporting a key role for this tissue in the synthesis and/or transport of metabolites involved in camptothecin synthesis.

Gene expression and metabolite analyses in roots of RNAi lines suggested the presence of one or more regulatory system influencing and balancing the production of indole and seco-iridoid precursors for MIA synthesis (Figures 9 and 10). Roots were the only tissue that specifically upregulated expression of the seco-iridoid genes *CYC1* and *G8O* in *TDC1*-RNAi plants [leading to accumulation of loganic acid (**2**)] and upregulated expression of *TDC1* in *CYC1*-RNAi [leading to accumulation of tryptamine (**4**)]. These data suggest a transcriptional regulatory mechanism that enhances flux of precursors from the indole and iridoid branches in roots, likely in response to cellular signals, indicating MIA synthesis is below a desired level. Such a system would permit *C. acuminata* to balance the production of indole and seco-iridoid precursors for export to aerial tissues or for use in maintaining a constitutive level of MIAs for defense against herbivore attack of roots. The simultaneous upregulation of *G8O* and *CYC1* in *TDC1*-RNAi roots (Figure 10A) and their clustering in coexpression analyses (Figure 5) with other seco-iridoid pathway candidates, including a putative ortholog of the *C. roseus* iridoid transcription factor BIS1, indicates that the pathway up to loganic acid synthesis is tightly coregulated. It seems plausible that in response to MIA deficiency in *TDC1*-RNAi roots that BIS1 or other transcription factors are impacted and mediate the observed effects on iridoid pathway transcripts. In transcriptome-wide coexpression analysis, *TDC1* and the seco-iridoid pathway genes were in separate clusters (Figure 5), indicating that the two branches are regulated in distinct ways. This is reinforced in targeted coexpression analyses using only transcripts from the seco-iridoid cluster in Figure 5 and MEP and tryptophan pathway enzymes, which provide IPP and tryptophan for iridoid and tryptamine synthesis. With few exceptions, transcripts from the three biochemical pathways cluster within their respective biosynthetic groups. Transcriptome analysis of various tissues from the RNAi lines is needed to gain a deeper understanding of the coordinated control of the tryptamine and iridoid branches in *C. acuminata.*

METHODS

Transcriptome Resources and Computational Analyses

The transcriptome profile for 53,154 unique *Camptotheca acuminata* transcripts was downloaded from the MPGR database where expression abundances are represented as FPKM (ftp://ftp.plantbiology.msu.edu/pub/data/MPGR/Camptotheca_acuminata/; Góngora-Castillo et al., 2012). The RNA-seq reads are available in the NCBI SRA under accession number SRP006330. Coexpression analyses were performed with the Multiexperiment Viewer software package (MeV v4.9) (Saeed et al., 2006) using $\log_2$-transformed FPKM expression values. Candidate genes identified in this study and their respective MPGR sequence numbers are given in Figure 5 and Supplemental Data Set S2.

To analyze the phylogenetic relationship of progesterone 5-β-reductase family members, the protein sequences for *C. acuminata* and *Rauvolfia serpentina* were derived from the following transcript sequences at http://medicinalplantgenomics.msu.edu and *Catharanthus roseus* sequences were searched in GenBank: *C. roseus*, KJ873882 (CrP5bR1), KJ873883 (CrP5bR2), KJ873884 (CrP5bR3), KJ873885 (CrP5bR4), KJ873886 (CrP5bR5, iridoid synthase), and KJ873887 (CrP5bR6); *C. acuminata*, KU842378 (CYC1), KU842379 (CYC2), GACF01077314, GACF01008548, GACF01024182, GACF01073333, and GACF01036291; and *R. serpentina*, GACE01080250, GACE01016867, GACE01082242, GACE01021747, GACE01073438, GACE01070053, GACE01001096, and GACE01023577. Protein sequences were aligned with ClustalW. A neighbor-joining tree was constructed with MEGA 6.06 (Tamura et al., 2011). The complete deletion option was used and bootstrap values determined from 1000 replicates and evolutionary distances computed using the Poisson correction method (Supplemental Figure 4 and Supplemental Data Set S4).

Amplification of the Coding Sequences for TDC1 and Putative Iridoid Synthases from *C. acuminata*

The open reading frames for *TDC1* and the putative iridoid synthases, *CYC1* and *CYC2*, were amplified by PCR with sequence-specific primers (Supplemental Table 2) from *C. acuminata* cDNA and the amplicons were then inserted into pENTR-SD/D (Life Technologies). The identities of the cloned fragments for *TDC1* (1513 bp), *CYC1* (1174 bp), and *CYC2* (1198 bp) were confirmed by sequencing.

Heterologous Expression and Purification of Recombinant Proteins

The full-length CYC1 and CYC2 coding sequences were cloned into the pDEST17 expression vector (Life Technologies). The *C. roseus* iridoid synthase (Geu-Flores et al., 2012) was also cloned into pDEST17. *Escherichia coli* Rosetta (DE3) cells harboring the pDEST17 constructs were grown at 37°C. Heterologous expression was induced with 0.5 mM isopropyl β-D-thiogalactopyranoside at an OD_{600} of 0.8. Cultures were then incubated at 16°C and cells were harvested after 8 or 16 h and lysed. The crude cell lysates were centrifuged at 20,000*g* and the His-tagged proteins in the supernatants were purified by Ni-chelating chromatography following manufacturer's instructions (Qiagen). The protein extracts were concentrated and the buffer was exchanged to 50 mM MOPS, pH 7.0, before storage at −80°C.

Dehydrogenase Activity and Iridoid Synthase Assays

Purified proteins were assayed for NAD(P)H dependent dehydrogenase activity using nitroblue tetrazolium chloride as electron acceptor, which when reduced, forms a dark blue formazan precipitate (Chigri et al., 2006). A 50-μL reaction mixture contained up to 4 μg protein, 200 μM NAD(P)H, and 80 μg nitroblue tetrazolium in 50 mM Tris HCl, pH 7.8. Control reactions were performed lacking NAD(P)H or protein.

8-Oxogeranial (**1**) was the generous gift of Sarah E. O'Connor and Nat Sherden (John Innes Centre, UK) and was synthesized from geraniol according to Geu-Flores et al. (2012) and contained a mixture of the two isomers 8-oxogeranial (**1**) and 8-oxoneral in an approximate ratio of 2:1. Reaction mixtures (100 μL total volume) contained 2.5 μg protein, 400 μM monoterpene substrate(s), and 400 μM NAD(P)H in 20 mM MOPS (pH 7.0) and were incubated for 1 h at room temperature. Assays were terminated and extracted with 200 μL dichloromethane. The reaction products were separated and analyzed by GC-MS in an Agilent 6890N system coupled to an Agilent 5973 MS detector. Chromatography was performed with an Agilent VF-5ms column (30 m × 0.25 mm × 0.25 μm plus 10 m EZ-Guard; part #CP9013) at 1.2 mL min^{-1} helium flow. The injection volume was 1 μL in splitless mode at an injector temperature of 250°C. The following oven program was used (run time 16.01 min): 1 min isothermal at 50°C, 20°C min^{-1} to 150°C, 45°C min^{-1} to 280°C, 4 min isothermal at 280°C, 40°C min^{-1} to 325°C, and 2 min isothermal at 325°C. The mass spectrometer was operated using 70 eV electron ionization mode with the following settings: solvent delay 2 min, resulting EM voltage 2141.2, ion source temperature at 230°C, and quadrupole temperature at 150°C. Mass spectra were recorded from *m/z* 30 to 600 at three spectrum/spectra.

Cloning and Construction of pHellsgate Constructs

To suppress expression of *TDC1* or *CYC1* in *C. acuminata*, 442- and 363-bp cDNA sequences, respectively, were amplified by PCR from the cloned full-length coding sequences. The amplicons were cloned into pENTR-D (Life Technologies) and then inserted into the binary vector pHellsgate12 (Helliwell and Waterhouse, 2005) and verified by restriction analyses and sequencing. The constructs were then transformed into *Agrobacterium tumefaciens* strain EHA105 (Hellens et al., 2000).

C. acuminata Cultivation and Generation of Transgenic RNAi Lines

Mature *C. acuminata* seeds were collected from trees growing in the San Antonio Zoo. Dehusked seeds were cleaned with 0.5% Tween 20 for at least 30 min, rinsed four to five times with distilled water, and then planted on 96-well flats with Redi-Earth Plug and Seedling Mix (Hummert International). Flats were kept in a growth room at 25°C ± 2°C under a 16-h photoperiod (100 μmol m^{-2} s^{-1}). Cotyledons from 3-week-old seedlings were used for Agrobacterium-mediated transformation with RNAi expression constructs. Seedlings were surface-sterilized using a 10% commercial bleach solution containing 0.1% Tween 20 for 10 min, then rinsed four times with sterile distilled water.

Agrobacterium EHA105 clones harboring a pHellsgate 12 construct were grown overnight at 28°C in Luria Bertani medium containing 25 μg/mL rifampicin and 50 μg/mL kanamycin. For infection, an Agrobacterium suspension (OD_{600} of 0.6) was made from an overnight culture using Lloyd and McCown liquid medium containing 100 μM acetosyringone. Prior to transformation, cotyledon sections were excised and precultured for 3 d in callus induction media (WPM Lloyd and McCown with vitamins) (Lloyd and McGown, 1981), 2% sucrose, 2 mg/L 1-naphthalene acetic acid, 2 mg/L 6-benzylaminopurine (BAP), pH 5.8, and 0.8% agar. Precultured explants were submerged in the Agrobacterium inoculum for 5 min and then transferred to fresh agar plates for 2 d at 25°C in the dark. Cotyledons were then transferred to fresh callus induction media supplemented with 500 mg/L carbenicillin and 100 mg/L cefotaxime for 6 to 7 days at 25°C ± 2°C under a 16-h photoperiod (70 μmol m^{-2} s^{-1}).

For selection of transformants, inoculated cotyledon explants were transferred to shoot induction and proliferation media WPM Lloyd and McCown (Lloyd, 1981) supplemented with 2% sucrose, 1 mg/L BAP, 0.3 mg/L indole-3-butyric acid, 500 mg/L carbenicillin, 100 mg/L cefotaxime, and 30 mg/L kanamycin. Subculture of explants to the same medium was performed every 2 to 3 weeks. Kanamycin-resistant shoots were excised and transferred to shoot elongation media (WPM Lloyd and McCown supplemented with 3% sucrose, 0.15 mg/L gibberellic acid, 0.15 mg/L BAP, 500 mg/L carbenicillin, 100 mg/L cefotaxime, and 30 mg/L kanamycin). Elongated shoots were rooted using shoot induction media supplemented with 1 mg/L indole-3-butyric acid. Plantlets with roots were then transferred to pots containing RediEarth soil mix and allowed to acclimate at 25°C ± 2°C under a 16-h photoperiod (100 μmol m^{-2} s^{-1}) for several weeks prior to transfer to greenhouse for further cultivation.

Real-Time Quantitative RT-PCR

Total RNA was extracted from 100 mg *C. acuminata* tissue by the hot-borate protocol (Birtić and Kranner, 2006). Prior to cDNA synthesis, the RNA extracts were treated with TURBO DNase (Ambion) to remove residual genomic DNA. cDNAs were synthesized from 1 μg of total RNA using SuperScript II reverse transcriptase (Life Technologies) and oligo$(dT)_{18}$ primer. qRT-PCRs were performed in triplicate in a Mastercycler RealPlex 2 (Eppendorf). Each 20-μL reaction contained 1× SYBR Green PCR Master Mix (Life Technologies) and forward and reverse primers (Supplemental Table 2) at a final concentration of 0.5 μM and 2 μL of 1:4 diluted *C. acuminata* cDNA. The following temperature profile was used for qRT-PCR analyses: 10 min at 95°C followed by 40 cycles with 15 s at 95°C and 1 min at 60°C. Single fragment amplification was verified by gel electrophoresis on a 3% agarose gel and visualization of the ethidium bromide stained DNA under UV light as well as by sequence analyses of PCR products from selected samples. Ct values were normalized to *ACTIN6*.

Metabolite Analyses in *C. acuminata* Nontransgenic and Transgenic Lines

For each sample, ~30 mg of frozen powdered plant tissue and 500 μL acetonitrile/water (7/3, v/v) containing 1.25 μM telmisartan (internal

standard) was added, vortexed for 5 s, and incubated in the dark at 4°C for 16 h. Samples were then centrifuged at 4°C and 10,000*g* for 30 min, supernatants were transferred to fresh tubes and centrifuged at 4°C and 10,000*g* for 15 min, and 40-μL aliquots were diluted by addition of 150 μL deionized water. Immediately prior to UHPLC/MS analysis, 10 μL of 10% formic acid was added by the autosampler to each extract and mixed by drawing the liquid into the autosampler syringe and ejecting back into the sample vial. This procedure minimized acid-catalyzed degradation while vials remained in the autosampler tray, and delivered metabolites to the column in an acidic solvent that improved chromatographic retention and resolution. Individual standard solutions of available standards tryptamine, loganic acid (ChromaDex), camptothecin (MP Biomedicals), and the internal standard telmisartan (Toronto Research Chemicals) were prepared over a range of concentrations from 0 to 70 μM and were analyzed together with each set of plant tissue extracts. Typical limits of detection were ~0.1 μM for each analyte, with a linear response of up to at least 50 μM in each case. UHPLC/MS analyses were performed using a Shimadzu LC-20AD ternary pump coupled to a SIL-5000 autosampler, column oven, and Waters LCT Premier mass spectrometer equipped with an electrospray ionization source. A 10-μL volume of each extract was analyzed using either a 52-min or a 15-min gradient elution method on an Ascentis Express C18 UHPLC column (2.1 × 100 mm, 2.7 μm) with mobile phases consisting of 10 mM ammonium formate in water, adjusted to pH 2.85 with formic acid (solvent A) and methanol (solvent B). The 52-min method gradient was as follows: 2% B at 0.00 to 2.00 min, linear gradient to 20% B at 20.00 min, linear gradient to 55% B at 43.00 min, then a step to 99% B at 43.01 min, then return to 2% B over 47.01 to 52.00 min. The 15-min method employed 8% B at 0.00 to 1.00 min, linear gradient to 40% B at 3.00 min, linear gradient to 70% B at 11.00 min, then step to 99% B at 11.01 and held until 13.00 min, followed by a return to 8% B and held from 14.00 to 15.00 min. For both gradients, the flow rate was 0.3 mL/min and the column temperature was 45°C. The mass spectrometer was operated using V optics in positive-ion mode with a typical resolution of ~4000 at full width at half maximum. Source parameters were as follows: capillary voltage 3200 V, sample cone voltage 10 V, desolvation temperature 350°C, source temperature 100°C, cone gas flow 40 L/h, and desolvation gas flow 350 L/h. Mass spectrum acquisition was performed in positive-ion mode over *m/z* 50 to 1500 with scan time of 0.1 s, using dynamic range extension. Mass spectra containing fragment ions were generated by rapid switching of aperture 1 voltage over four parallel data acquisition functions (20, 40, 60, and 80 V) (Gu et al., 2010). The lowest aperture 1 voltage yielded negligible in-source fragmentation for all metabolites except the iridoid glycosides loganic acid and secologanic acid, which, in addition to $[M+H]^+$ and $[M+\text{alkali metal}]^+$ ions, also yielded ions corresponding to neutral loss of the glucose moiety (162 D). Accurate masses and fragments were confirmed in UHPLC/MS/MS analyses (Xevo G2-S and G2-XS QTOF mass spectrometers; Waters) using four scan functions (method A: 10, 20, 40, and 60 V) or a collision energy ramp (method B, from 10 to 50 V for *m/z* 200 to 15 to 80 V at *m/z* 1000) (Table 1; Supplemental Table 1).

For quantitative analyses, the 15-min gradient UHPLC/MS method was used. The extracted ion chromatograms for each target analyte were integrated, and analytes were quantified, using QuanLynx tool (Waters) with a mass window allowance of 0.2. Sodium adduct peaks $[M+Na]^+$ and $[M+H]^+$ were quantified for carboxylic acids and downstream metabolites, respectively. All calculated peak areas were normalized to the peak area for the internal standard telmisartan and tissue fresh weight.

Separation of loganic acid and secologanic acid isomers was obtained by using a 31-min gradient elution method on an Agilent ZORBAX Eclipse XDB C8 HPLC column (4.6 × 150 mm, 5 μm) with mobile phases consisting of 0.1% v/v formic acid in water (solvent A) and acetonitrile (solvent B). The elution gradient was: 5% B at 0.00 to 1.00 min, linear increase to 10% B at 3.00 min, linear to 30% B at 25.00 min, followed by a rapid increase from 30 to 99% B over 25.00 to 26.00 min, hold at 99% B over 26.01 to 28.00 min, then return to 5% B and held over 29.00 to 31.00 min. The flow rate was 1.0 mL/min and the column temperature was 30°C. Loganic acid isomer 1, loganic acid isomer 2, secologanic acid isomer 1, and isomer 2 eluted at 5.2 min, 6.1 min, 8.2 min, and 8.6 min, respectively.

NMR Characterization of Strictosidinic Acid Isomers

Young leaf tissue (350 g fresh weight) was freshly harvested from greenhouse-cultivated *C. acuminata* plants, transferred to a 4-liter amber glass bottle, and extracted using 2 liters of HPLC grade acetonitrile for 16 h at 4°C. The extract was ultrasonicated for 2 min followed by liquid-liquid partitioning against two volumes of 500 mL hexane. The lower acetonitrile layer was collected, and solvent was removed under reduced pressure in a rotary evaporator and reconstituted in 10 mL of methanol/water (5/95 v/v) immediately before UHPLC/MS metabolite profiling. UHPLC/MS metabolite profiling was performed using a Shimadzu LC-20AD ternary pump coupled to a SIL-5000 autosampler, column oven, and Waters LCT Premier mass spectrometer equipped with an electrospray ionization source and operated in positive-ion mode. Preparative HPLC fractionation was performed using a Waters Model 2795 HPLC system coupled to a LKB BROMMA 221 fraction collector. An Ascentis Express F5 (pentafluorophenylpropyl) column (4.6 × 150 mm, 2.7 μm particles; Supelco Sigma-Aldrich) was used with a solvent flow rate of 0.8 mL/min for profiling and preparative fractionation. The flow was split postcolumn, and ~0.3 mL/min was diverted to the mass spectrometer. The mobile phase consisted of water (Solvent A) and methanol (Solvent B) using linear gradients: 10% B during 0 to 1 min, to 30% B at 2 min, to 50% B at 14 min, to 65% B at 15 min, to 90% B at 25 min, then 90 to 99% B over 25 to 32 min followed by a hold until 36 min, then return to 10% B over 36.01 to 40 min. Fractions were collected at 15-s intervals, and 50 injections of 150 μL were made to accumulate sufficient material for NMR analysis. Two major strictosidinic acid isomers, denoted isomers 2 and 3 based on the order of their elution times on the C18 column, were collected in fractions 60-66 and 42-46, respectively, from the F5 column. Fractions for each isomer were combined, dried under reduced pressure and reconstituted in CD_3OD. NMR spectra (^1H, J-resolved ^1H, ^1H-^1H COSY, HSQC, cHSQC, HMBC) were recorded on a 21.1 T Bruker Avance-900 NMR spectrometer equipped with a TCI inverse triple-resonance cryoprobe at 900 MHz (^1H) and 225 MHz (^{13}C) at the Michigan State University Max T. Rogers NMR Facility. Additional NMR data are presented in Supplemental Table 3 and Supplemental Data Set S1.

In Vivo Labeling Studies of *C. acuminata* Apical Cuttings

Shoot cuttings of ~20 cm in length were taken from ~1-year-old wild-type and *TDC1*-RNAi plants. Shoots were incubated individually in 15-mL conical tubes containing 100 μM [α,α,β,β-d_4]-tryptamine (CDN Isotopes, 97% isotopic enrichment) and 10 to 15 mg carbenicillin in 10 mL water at room temperature under continuous light (25 μmol m^{-2} s^{-1}). Controls were similarly treated without addition of deuterated tryptamine. Six biological replicates were performed for each treatment. The water level was regularly adjusted with water or 100 μM deuterated tryptamine solution as needed. After 6 weeks, stems and leaves were harvested separately, frozen with liquid nitrogen, and analyzed as described above using the 52-min UHPLC/MS method.

Accession Numbers

C. acuminata sequence data from this article can be found in the GenBank/EMBL data libraries under the following accession numbers: KU842377 (*TDC1*), KU842378 (*CYC1*, iridoid synthase), and KU842379 (*CYC2*, progesterone 5-β-reductase like). All MPGR sequence data were previously deposited in GenBank (Góngora-Castillo et al., 2012), and relevant accession numbers are listed in Supplemental Data Set S2.

Supplemental Data

Supplemental Figure 1. Loganic acid isomers in *C. acuminata*.

Supplemental Figure 2. Secologanic acid isomers in *C. acuminata*.

Supplemental Figure 3. Heat map of expression data for candidate genes in the tryptamine and seco-iridoid branch of the camptothecin pathway.

Supplemental Figure 4. Phylogenetic relationship of progesterone 5-β-reductase family members from *C. acuminata*, *C. roseus*, and *R. serpentina*.

Supplemental Figure 5. Colorimetric dehydrogenase assay with the purified recombinant proteins CYC1, CYC2, and *C. roseus* iridoid synthase.

Supplemental Figure 6. *C. acuminata* wild type and two RNAi lines.

Supplemental Table 1. Relevant compounds detected in wild-type *C. acuminata*.

Supplemental Table 2. List of primers used in this study.

Supplemental Table 3. NMR metadata.

Supplemental Data Set S1. NMR spectra.

Supplemental Data Set S2. Accession numbers and sequence identities of *C. acuminata* candidate genes involved in the synthesis of indole and monoterpene components.

Supplemental Data Set S3. FPKM values.

Supplemental Data Set S4. Alignment of the amino acid sequences of progesterone 5-β-reductase family members from *C. acuminata*, *C. roseus*, and *R. serpentina*.

ACKNOWLEDGMENTS

We thank Sarah E. O'Connor and Nat Sherden (John Innes Centre, UK) for sharing the *C. roseus* iridoid synthase expression construct and 8-oxogeranial, Thomas McKnight (Texas A&M University) for providing us with *C. acuminata* seeds collected from trees at the San Antonio Zoo, and Evan Klug and Alexandra Palmiter for technical assistance. Tandem mass spectra were collected using the Waters QTof instruments at the Michigan State University Mass Spectrometry and Metabolomics Core. A.D.J. acknowledges support from Michigan AgBioResearch project MICL-02143 and D.D.P. and A.D.J. from the National Institute of General Medical Sciences Project 1RC2GM092521.

AUTHOR CONTRIBUTIONS

R.S., D.D.P., and A.D.J. designed the research. R.S., M.M.-L., S.P., V.S., and A.M. performed the research. R.S., S.P., and V.S. analyzed data. R.S., D.D.P., and A.D.J. wrote the article.

Received March 7, 2016; revised June 20, 2016; accepted July 9, 2016; published July 18, 2016.

REFERENCES

Aberham, A., Pieri, V., Croom, E.M., Jr., Ellmerer, E., and Stuppner, H. (2011). Analysis of iridoids, secoiridoids and xanthones in *Centaurium erythraea, Frasera caroliniensis* and *Gentiana lutea* using LC-MS and RP-HPLC. J. Pharm. Biomed. Anal. **54:** 517–525.

Aimi, N., Nishimura, M., Miwa, A., Hoshino, H., Sakai, S., and Haginiwa, J. (1989). Pumiloside and deoxypumiloside; plausible intermediate of camptothecin biosynthesis. Tetrahedron Lett. **30:** 4991–4994.

Ajala, O.S., Piggott, A.M., Plisson, F., Khalil, Z., Huang, X., Adesegun, S.A., Coker, H.A.B., and Capon, R.J. (2011). Ikirydinium A: a new indole alkaloid from the seeds of *Hunteria umbellata* (K. Schum). Tetrahedron Lett. **52:** 7125–7127.

Arbain, D., Putra, D.P., and Sargent, M.V. (1993). The alkaloids of *Ophiorrhiza filistipula.* Aust. J. Chem. **46:** 977–985.

Asada, K., Salim, V., Masada-Atsumi, S., Edmunds, E., Nagatoshi, M., Terasaka, K., Mizukami, H., and De Luca, V. (2013). A 7-deoxyloganetic acid glucosyltransferase contributes a key step in secologanin biosynthesis in Madagascar periwinkle. Plant Cell **25:** 4123–4134.

Asano, T., Kobayashi, K., Kashihara, E., Sudo, H., Sasaki, R., Iijima, Y., Aoki, K., Shibata, D., Saito, K., and Yamazaki, M. (2013). Suppression of camptothecin biosynthetic genes results in metabolic modification of secondary products in hairy roots of *Ophiorrhiza pumila.* Phytochemistry **91:** 128–139.

Bedewitz, M.A., et al. (2014). A root-expressed L-phenylalanine: 4-hydroxyphenylpyruvate aminotransferase is required for tropane alkaloid biosynthesis in *Atropa belladonna.* Plant Cell **26:** 3745–3762.

Birtić, S., and Kranner, I. (2006). Isolation of high-quality RNA from polyphenol-, polysaccharide- and lipid-rich seeds. Phytochem. Anal. **17:** 144–148.

Bracher, D., and Kutchan, T.M. (1992). Strictosidine synthase from *Rauvolfia serpentina*: analysis of a gene involved in indole alkaloid biosynthesis. Arch. Biochem. Biophys. **294:** 717–723.

Cardoso, C.L., Castro-Gamboa, I., Silva, D.H., Furlan, M., Epifanio, Rde.A., Pinto, Ada.C., Moraes de Rezende, C., Lima, J.A., and Bolzani, Vda.S. (2004). Indole glucoalkaloids from *Chimarrhis turbinata* and their evaluation as antioxidant agents and acetylcholinesterase inhibitors. J. Nat. Prod. **67:** 1882–1885.

Carte, B.K., DeBrosse, C., Eggleston, D., Hemling, M., Mentzer, M., Poehland, B., Troupe, N., Westley, J.W., and Hecht, S.M. (1990). Isolation and characterization of a presumed biosynthetic precursor of camptothecin from extracts of *Camptotheca acuminata.* Tetrahedron **46:** 2747–2760.

Chigri, F., Hörmann, F., Stamp, A., Stammers, D.K., Bölter, B., Soll, J., and Vothknecht, U.C. (2006). Calcium regulation of chloroplast protein translocation is mediated by calmodulin binding to Tic32. Proc. Natl. Acad. Sci. USA **103:** 16051–16056.

Courdavault, V., Papon, N., Clastre, M., Giglioli-Guivarc'h, N., St-Pierre, B., and Burlat, V. (2014). A look inside an alkaloid multisite plant: the *Catharanthus* logistics. Curr. Opin. Plant Biol. **19:** 43–50.

De Luca, V., Marineau, C., and Brisson, N. (1989). Molecular cloning and analysis of cDNA encoding a plant tryptophan decarboxylase: comparison with animal dopa decarboxylases. Proc. Natl. Acad. Sci. USA **86:** 2582–2586.

De Luca, V., Salim, V., Thamm, A., Masada, S.A., and Yu, F. (2014). Making iridoids/secoiridoids and monoterpenoid indole alkaloids: progress on pathway elucidation. Curr. Opin. Plant Biol. **19:** 35–42.

Fan, G., Luo, W.Z., Luo, S.H., Li, Y., Meng, X.L., Zhou, X.D., and Zhang, Y. (2014). Metabolic discrimination of *Swertia mussotii* and *Swertia chirayita* known as "Zangyinchen" in traditional Tibetan medicine by (1)H NMR-based metabolomics. J. Pharm. Biomed. Anal. **98:** 364–370.

Farias, F.M., Passos, C.S., Arbo, M.D., Barros, D.M., Gottfried, C., Steffen, V.M., and Henriques, A.T. (2012). Strictosidinic acid, isolated from *Psychotria myriantha* Mull. Arg. (Rubiaceae), decreases serotonin levels in rat hippocampus. Fitoterapia **83:** 1138–1143.

Geu-Flores, F., Sherden, N.H., Courdavault, V., Burlat, V., Glenn, W.S., Wu, C., Nims, E., Cui, Y., and O'Connor, S.E. (2012). An

alternative route to cyclic terpenes by reductive cyclization in iridoid biosynthesis. Nature **492:** 138–142.

Góngora-Castillo, E., et al. (2012). Development of transcriptomic resources for interrogating the biosynthesis of monoterpene indole alkaloids in medicinal plant species. PLoS One **7:** e52506.

Gopalakrishnan, R., and Shankar, B. (2014). Multiple shoot cultures of *Ophiorrhiza rugosa* var. decumbens Deb and Mondal–a viable renewable source for the continuous production of bioactive *Camptotheca* alkaloids apart from stems of the parent plant of *Nothapodytes foetida* (Wight) Sleumer. Phytomedicine **21:** 383–389.

Graikou, K., Aligiannis, N., Chinou, I.B., and Harvala, C. (2002). Cantleyoside-dimethyl-acetal and other iridoid glucosides from *Pterocephalus perennis*–antimicrobial activities. Z. Naturforsch., C, J. Biosci. **57:** 95–99.

Gu, L., Jones, A.D., and Last, R.L. (2010). Broad connections in the *Arabidopsis* seed metabolic network revealed by metabolite profiling of an amino acid catabolism mutant. Plant J. **61:** 579–590.

Hamzah, A.S., Arbain, D., Sargent, M.M.V., and Lajis, N.H. (1994). The alkaloids of *Ophiorrhiza communis* and *O. tomentosa*. Pertanika J. Sci. Tech. **2:** 33–38.

Han, Q.B., Li, S.L., Qiao, C.F., Song, J.Z., Cai, Z.W., Pui-Hay But, P., Shaw, P.C., and Xu, H.X. (2008). A simple method to identify the unprocessed *Strychnos* seeds used in herbal medicinal products. Planta Med. **74:** 458–463.

Hellens, R., Mullineaux, P., and Klee, H. (2000). Technical Focus: a guide to *Agrobacterium* binary Ti vectors. Trends Plant Sci. **5:** 446–451.

Helliwell, C.A., and Waterhouse, P.M. (2005). Constructs and methods for hairpin RNA-mediated gene silencing in plants. Methods Enzymol. **392:** 24–35.

Höfer, R., Dong, L., André, F., Ginglinger, J.F., Lugan, R., Gavira, C., Grec, S., Lang, G., Memelink, J., Van der Krol, S., Bouwmeester, H., and Werck-Reichhart, D. (2013). Geraniol hydroxylase and hydroxygeraniol oxidase activities of the CYP76 family of cytochrome P450 enzymes and potential for engineering the early steps of the (seco)iridoid pathway. Metab. Eng. **20:** 221–232.

Hutchinson, C.R., Heckendorf, A.H., Straughn, J.L., Daddona, P.E., and Cane, D.E. (1979). Biosynthesis of camptothecin. 3. Definition of strictosamide as the penultimate biosynthetic precursor assisted by carbon-13 and deuterium NMR spectroscopy. J. Am. Chem. Soc. **101:** 3358–3369.

Irmler, S., Schröder, G., St-Pierre, B., Crouch, N.P., Hotze, M., Schmidt, J., Strack, D., Matern, U., and Schröder, J. (2000). Indole alkaloid biosynthesis in *Catharanthus roseus*: new enzyme activities and identification of cytochrome P450 CYP72A1 as secologanin synthase. Plant J. **24:** 797–804.

Itoh, A., Tanaka, Y., Nagakura, N., Akita, T., Nishi, T., and Tanahashi, T. (2008). Phenolic and iridoid glycosides from *Strychnos axillaris.* Phytochemistry **69:** 1208–1214.

Kumar, K., Kumar, S.R., Dwivedi, V., Rai, A., Shukla, A.K., Shanker, K., and Nagegowda, D.A. (2015). Precursor feeding studies and molecular characterization of geraniol synthase establish the limiting role of geraniol in monoterpene indole alkaloid biosynthesis in *Catharanthus roseus* leaves. Plant Sci. **239:** 56–66.

Leménager, D., Ouelhazi, L., Mahroug, S., Veau, B., St-Pierre, B., Rideau, M., Aguirreolea, J., Burlat, V., and Clastre, M. (2005). Purification, molecular cloning, and cell-specific gene expression of the alkaloid-accumulation associated protein CrPS in *Catharanthus roseus.* J. Exp. Bot. **56:** 1221–1228.

Liu, Y.-Q., Li, W.-Q., Morris-Natschke, S.L., Qian, K., Yang, L., Zhu, G.-X., Wu, X.-B., Chen, A.-L., Zhang, S.-Y., Nan, X., and Lee, K.-H. (2015). Perspectives on biologically active camptothecin derivatives. Med. Res. Rev. **35:** 753–789.

Lloyd, G., and McGown, B. (1981). Commercially-feasible micropropagation of Mountain Laurel, *Kalmia latifolia*, by shoot tip culture. Proc. Int. Plant Prop. Soc. **30:** 421–427.

López-Meyer, M., and Nessler, C.L. (1997). Tryptophan decarboxylase is encoded by two autonomously regulated genes in *Camptotheca acuminata* which are differentially expressed during development and stress. Plant J. **11:** 1167–1175.

Lorence, A., and Nessler, C.L. (2004). Camptothecin, over four decades of surprising findings. Phytochemistry **65:** 2735–2749.

Marquez, B.L., Gerwick, W.H., and Williamson, R.T. (2001). Survey of NMR experiments for the determination of ^{n}J(C,H) heteronuclear coupling constants in small molecules. Magn. Reson. Chem. **39:** 499–530.

Miettinen, K., et al. (2014). The seco-iridoid pathway from *Catharanthus roseus*. Nat. Commun. **5:** 3606.

Montoro, P., Maldini, M., Piacente, S., Macchia, M., and Pizza, C. (2010). Metabolite fingerprinting of *Camptotheca acuminata* and the HPLC-ESI-MS/MS analysis of camptothecin and related alkaloids. J. Pharm. Biomed. Anal. **51:** 405–415.

Müller, A.A., and Weigend, M. (1998). Iridoids from *Loasa acerifolia.* Phytochemistry **49:** 131–135.

Munkert, J., Pollier, J., Miettinen, K., Van Moerkercke, A., Payne, R., Müller-Uri, F., Burlat, V., O'Connor, S.E., Memelink, J., Kreis, W., and Goossens, A. (2015). Iridoid synthase activity is common among the plant progesterone 5β-reductase family. Mol. Plant **8:** 136–152.

Murata, J., Roepke, J., Gordon, H., and De Luca, V. (2008). The leaf epidermome of *Catharanthus roseus* reveals its biochemical specialization. Plant Cell **20:** 524–542.

Patthy-Lukáts, Á., Károlyházy, L., Szabó, L.F., and Podányi, B. (1997). First direct and detailed stereochemical analysis of strictosidine. J. Nat. Prod. **60:** 69–75.

Rastrelli, L., Caceres, A., Morales, C., De Simone, F., and Aquino, R. (1998). Iridoids from *Lippia graveolens.* Phytochemistry **49:** 1829–1832.

Reanmongkol, W., Subhadhirasakul, S., Kongsang, J., Tanchong, M., and Kitti, J. (2000). Analgesic and antipyretic activities of n-butanol alkaloids extracted from the stem bark *Hunteria Zeylanica* and its major constituent, strictosidinic acid, in mice. Pharm. Biol. **38:** 68–73.

Saeed, A.I., Bhagabati, N.K., Braisted, J.C., Liang, W., Sharov, V., Howe, E.A., Li, J., Thiagarajan, M., White, J.A., and Quackenbush, J. (2006). TM4 microarray software suite. Methods Enzymol. **411:** 134–193.

Salim, V., Wiens, B., Masada-Atsumi, S., Yu, F., and De Luca, V. (2014). 7-deoxyloganetic acid synthase catalyzes a key 3 step oxidation to form 7-deoxyloganetic acid in *Catharanthus roseus* iridoid biosynthesis. Phytochemistry **101:** 23–31.

Salim, V., Yu, F., Altarejos, J., and De Luca, V. (2013). Virus-induced gene silencing identifies *Catharanthus roseus* 7-deoxyloganic acid-7-hydroxylase, a step in iridoid and monoterpene indole alkaloid biosynthesis. Plant J. **76:** 754–765.

Serrilli, A.M., Ramunno, A., Amicucci, F., Chicarella, V., Santoni, S., Ballero, M., Serafini, M., and Bianco, A. (2008). Iridoidic pattern in endemic Sardinian plants: the case of *Galium* species. Nat. Prod. Res. **22:** 618–622.

Sheriha, G.M., and Rapoport, H. (1976). Biosynthesis of *Camptotheca acuminata* alkaloids. Phytochemistry **15:** 505–508.

Skaltsounis, A.L., Tillequin, F., Koch, M., Pusset, J., and Chauvière, G. (1989). Iridoids from *Scaevola racemigera*. Planta Med. **55:** 191–192.

Tamura, K., Peterson, D., Peterson, N., Stecher, G., Nei, M., and Kumar, S. (2011). MEGA5: molecular evolutionary genetics analysis

using maximum likelihood, evolutionary distance, and maximum parsimony methods. Mol. Biol. Evol. **28:** 2731–2739.

Van Moerkercke, A., et al. (2015). The bHLH transcription factor BIS1 controls the iridoid branch of the monoterpenoid indole alkaloid pathway in *Catharanthus roseus.* Proc. Natl. Acad. Sci. USA **112:** 8130–8135.

Wall, M.E., Wani, M.C., Cook, C.E., Palmer, K.H., McPhail, A.T., and Sim, G.A. (1966). Plant antitumor agents. I. The isolation and structure of camptothecin, a novel alkaloidal leukemia and tumor inhibitor from *Camptotheca acuminata.* J. Am. Chem. Soc. **88:** 3888–3890.

Wink, M. (2003). Evolution of secondary metabolites from an ecological and molecular phylogenetic perspective. Phytochemistry **64:** 3–19.

Wright, C.M., van der Merwe, M., DeBrot, A.H., and Bjornsti, M.-A. (2015). DNA topoisomerase I domain interactions impact enzyme activity and sensitivity to camptothecin. J. Biol. Chem. **290:** 12068–12078.

Yamazaki, M., et al. (2013). Coupling deep transcriptome analysis with untargeted metabolic profiling in *Ophiorrhiza pumila* to further the understanding of the biosynthesis of the anti-cancer alkaloid camptothecin and anthraquinones. Plant Cell Physiol. **54:** 686–696.

Yamazaki, Y., Sudo, H., Yamazaki, M., Aimi, N., and Saito, K. (2003a). Camptothecin biosynthetic genes in hairy roots of *Ophiorrhiza pumila*: cloning, characterization and differential expression in tissues and by stress compounds. Plant Cell Physiol. **44:** 395–403.

Yamazaki, Y., Urano, A., Sudo, H., Kitajima, M., Takayama, H., Yamazaki, M., Aimi, N., and Saito, K. (2003b). Metabolite profiling of alkaloids and strictosidine synthase activity in camptothecin producing plants. Phytochemistry **62:** 461–470.

Zhang, T., Li, J., Li, B., Chen, L., Yin, H.L., Liu, S.J., Tian, Y., and Dong, J.X. (2012). Two novel secoiridoid glucosides from *Tripterospermum chinense.* J. Asian Nat. Prod. Res. **14:** 1097–1102.

Zhou, Z., Yin, W., Zhang, H., Feng, Z., and Xia, J. (2013). A new iridoid glycoside and potential MRB inhibitory activity of isolated compounds from the rhizomes of *Cyperus rotundus* L. Nat. Prod. Res. **27:** 1732–1736.

Ziegler, J., and Facchini, P.J. (2008). Alkaloid biosynthesis: metabolism and trafficking. Annu. Rev. Plant Biol. **59:** 735–769 (Review).